Nanotechnol Rev 1 (2012): 213–233 © 2012 by Walter de Gruyter • Berlin • Boston. DOI 10.1515/ntrev-2011-0008

Nanofabricated plasmonic nano-bio hybrid structures in biomedical detection

Wenwei Zheng[1,2], Heather C. Chiamori[3,4], Gang Logan Liu[2,5], Liwei Lin[3,4] and Fanqing Frank Chen[2,*]

[1] Department of Nutritional Science and Toxicology, University of California, Berkeley, CA 94720, USA
[2] Life Sciences Division, Lawrence Berkeley National Laboratory, Berkeley, CA 94720, USA, e-mail: f_chen@lbl.gov
[3] Department of Mechanical Engineering, University of California, Berkeley, CA 94720, USA
[4] Berkeley Sensor and Actuator Center, Berkeley, CA 94720, USA
[5] Micro and Nanotechnology Laboratory, Department of Electrical and Computer Engineering, University of Illinois at Urbana-Champaign, Urbana, IL 61801, USA

*Corresponding author

Abstract

Our study of biological systems increasingly depends on our ability to dynamically and quantitatively measure the molecular processes with high sensitivity, speed, flexibility, multiplexity, throughput, and reproducibility, usually within the context of a complex biological and chemical mixture of tiny amount. To address these major challenges, plasmon-resonant nanostructure biomolecule hybrids (nano-bio hybrids), so-called plasmonic nanobiosensors, are being developed and viewed as one key breakthrough area for real-time and parallelized biomedical analysis with high sensitivity and selectivity. Hereby, we present a solution of integrated plasmonic system by synergizing three core techniques: (i) nanoplasmonics that manipulates electromagnetic radiation (light) at dielectric-metal interfaces by tuning properties of nanomaterials, (ii) nanofabrication and controlled synthesis of nanomaterials containing noble metals (e.g., Au, Ag, Pt, and Cu), and (iii) bioconjugates techniques that modify surface of nanomaterials with various bioprobes (e.g., antibodies, enzymes, aptamers, and molecular imprint polymers). Applications of these plasmonic nano-bio hybrid structures are also discussed.

Keywords: genomic sensing; localized surface plasmon spectroscopy (LSPR); nano-bio hybrids; plasmonic nano-resonance; plasmonic structures; proteomic sensing; surface-enhanced Raman spectroscopy (SERS); surface enhancements; surface plasmons.

1. Introduction

In view of basic science, to understand biological systems increasingly depends on our ability to dynamically and quantitatively measure the molecular processes with high sensitivity, speed, flexibility, multiplexity, throughput, and reproducibility, usually within the context of a complex biological and chemical mixture of tiny amount. A living cell responds to its changing environment both inside and outside itself in such a dynamic way that hundreds and thousands of signaling proteins, enzymes, siRNA, DNA, mRNA, and transcription and translation factors are constantly modified or synthesized, transferred from one organelle to another, and perform appropriate cell functions in macromolecule complexes, behaving like an army of molecular machines working in perfect synchronicity and harmony. These biomolecular complexes are not only heterogeneously distributed, recombined, modified, and reassembled continuously, but perpetually changed over time with the change of surrounding microenvironments [1]. To quantitatively follow the biochemical reactions within multi-molecule complexes, it is vital for the general goal of intimately following molecular machines in cell signaling, growth, differentiation, apoptosis, cell developmental processes, and relevant diseases. In the biotechnology industry, combinatorial methods are increasingly applied to synthesize new biocatalysts or drugs, demanding simultaneous analysis of thousands of pathogens, mutants, drug target enzymes, or therapeutic drugs themselves. Furthermore, in personalized medicine, as dictated by economic reasons, mass application of screening and diagnostic tools have to be fast, convenient, and low-cost, requiring miniaturization, parallelization, integration, as well as automation of biosensing devices.

To address these major challenges, the best hope lies in cutting edge biosensing research. Among all the biosensors, plasmon-resonant nanostructure biomolecule hybrids (nano-bio hybrids), so-called plasmonic nanobiosensors [2, 3], are being developed and viewed as one key breakthrough area for real-time and parallelized biomedical analysis with high sensitivity and selectivity. Hereby, we present a solution of integrated plasmonic system by synergizing three core techniques: (i) plasmonics that manipulates electromagnetic radiation (light) at dielectric-metal interfaces by tuning properties of nanomaterials, (ii) nanofabrication and controlled synthesis of nanomaterials containing metals (e.g., Au, Ag, Pt, and Cu), and (iii) bioconjugates techniques that modify surface of nanomaterials with various bioprobes (e.g., antibodies, enzymes, aptamers [4, 5], and molecular imprint polymers [6]). Biomaterials such as proteins, DNA, or RNA, have dimensions of 2–20 nm, similar to those of plasmonic nanostructures, thus, the two classes of material are structurally compatible. Plasmonic

Brought to you by | University of California - Berkeley (University of California - Berkeley)
Authenticated | 172.16.1.226
Download Date | 7/6/12 12:05 PM

nanomaterials exhibit unique electronic, photonic, and catalytic properties, providing electronic or optical transduction of biological phenomena, whereas biomaterials have unique recognition and catalytic properties. Their integration yields plasmonic nano-bio hybrid sensors with multiple synergetic advantages over traditional molecular imaging techniques: sensitivity, stability, biocompatibility, selectivity, and spectroscopic imaging capability. Furthermore, recently, significant advancements in controlled synthesis and nanofabrication [7–9], theory and electrodynamic modeling of optical properties [10–12], and surface functionalization [13–15] of plasmonic nanomaterials greatly enhance the ability to control and tune the unique optical and electronic properties of plasmonic nanostructures through their sizes, structures, composition, and shapes, enabling the utilization of huge libraries of probes for different analytes in formats such as microarray, microfluidics, MEMS, etc. Thus, plasmonic nanobiosensors promise a great potential in the development of high-throughput techniques for the parallel analysis of multiple components in samples.

These recent advancements in nanotechnology and nanoplasmonics also enable hybrid plasmonic nanostructures as powerful subnanometer and nanometer tools to directly interface with intracellular processes. The plasmonic nanobiosensors focus electromagnetic fields to significantly enhance spectral information for localized surface plasmon spectroscopy (LSPR) [16, 17], surface-enhanced Raman spectroscopy (SERS) [18, 19], plasmon resonance energy transfer (PRET) [20–22], and integrated photoacoustic-photothermal contrast agents [23]. In this way, we can obtain quantitative spectral snapshots of the complex biochemical reaction over time as a result of local biochemistry-induced plasmonic changes. In this review, we will discuss nanoplasmonic theory, summarize major nanosynthesis and nanofabrication techniques, and describe surface functionalization of plasmonic nanobiosensors. We will then give examples of the applications and summarize the synergetic relationships among these three core techniques contained in plasmonic nanobiosensing to address the major aforementioned challenges in biosensing research.

2. Theoretical background

Nanophotonics is defined as “the science and engineering of light matter interactions that take place on wavelength and subwavelength scales where the physical, chemical or structural nature of natural or artificial nanostructured matter controls the interactions” [24]. One of the major subfields of nanophotonics is plasmonics, in which manipulation of light is based on interaction processes between electromagnetic radiation and free-electron plasma (or conduction electrons) at dielectric-metal planar interfaces or nanocurved interfaces, resulting in surface plasmon-polaritons (SPPs) or localized surface plasmon-polaritons (LSPs) [25], respectively. A plasmon is a quantum quasi-particle representing the elementary excitations, or modes, of the charge density oscillations in a free-electron plasma [26]. As shown in Figure 1A, SPPs are

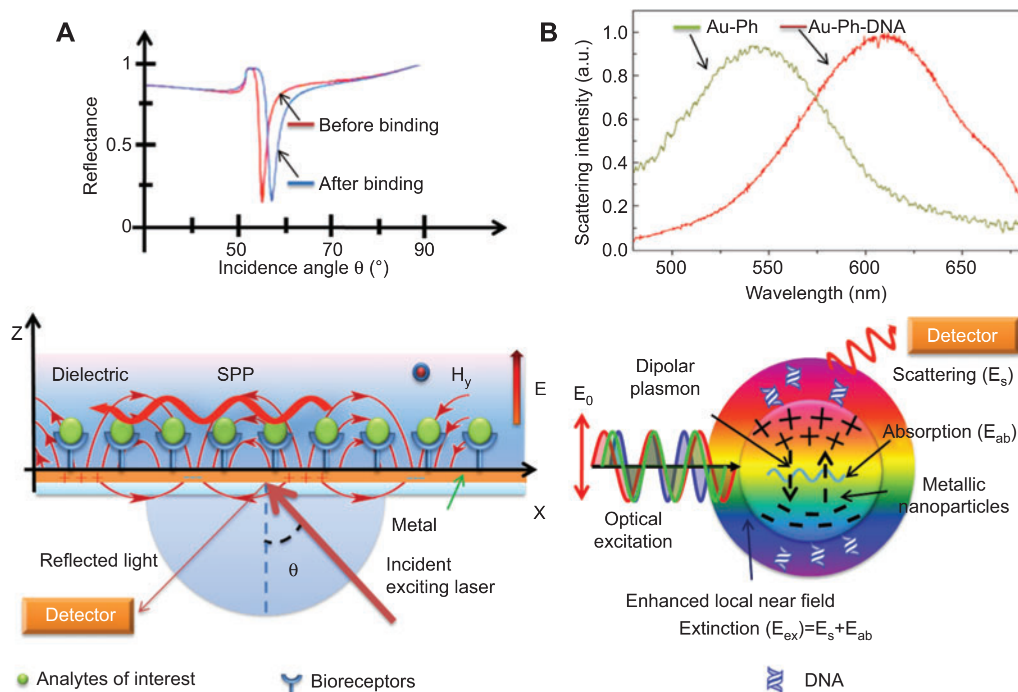

Figure 1 Illustration of (A) a typical experiment setup (bottom) using surface plasmon polaritons (or propagating plasmon) and a resulting reflectivity spectrum (top) obtained in an angle-solved mode and (B) a typical measurement setup (bottom) using localized surface plasmons to reflect the DNA binding on gold nanoparticles can dramatically shift the scattering peak wavelength of a single gold nanoparticle, and a resulting scattering spectrum in biosensing (top) [27]. Au-Ph are phosphine-coated Au nanoparticles, where phosphine acts as a surfactant to solubilize uncoated Au nanoparticle in aqueous solution.

Brought to you by | University of California - Berkeley (University of California - Berkeley)
Authenticated | 172.16.1.226
Download Date | 7/6/12 12:05 PM

propagating dispersive electromagnetic (EM) waves coupled to the electron plasma of a conductor at the planar interface between dielectric and metal materials, having a combined EM wave and surface charge character. The surface charge is generated by the electric field normal to the surface, whereas the EM waves propagate in the *x*-direction (**H** is in the *y*-direction, Figure 1A) for distances on the order of tens to hundreds of microns. This combined character leads to the field component normal to the surface enhanced near the surface and decaying exponentially with distance in the *z*-direction on the order of 10–200 nm (Figure 1A) [28–30]. The enhancement reaches its maximum when SPPs resonate with the incident exciting laser, which is called surface plasmon resonance (SPR), corresponding to the minimum reflectivity as shown in Figure 1A.

Localized surface plasmon-polaritons are non-propagating collective oscillations of the conduction electrons of metallic nanostructures against the background of cationic metal cores [31] coupled to the incident exciting EM field (light) (Figure 1B). For a particle much smaller than the wavelength of the exciting light, the dipolar plasmon is dominant in the oscillation, which contains an effective restoring force on the driven electrons. When the exciting laser light is in resonance with the dipolar plasmon, the metal particle will radiate light characterized by dipolar radiation [32], leading to electrical field (E) amplification both inside and in the near-field zone outside the particle. This resonance is called the localized surface plasmon resonance (LSPR). Typical materials for plasmonic applications are noble metals, particularly silver or gold. Silver displays sharper and more intense LSPR bands than gold, whereas gold nanostructures are chemically more stable and biologically more compatible than silver.

The plasmon resonance modes depend on the dielectric constants of the metallic nanoparticle and the surrounding material. Within the optical frequency range, the complex dielectric constants ε ($\varepsilon=\varepsilon'+i\varepsilon''$) or the permittivity of the metallic materials, such as gold and silver, changes rapidly with the light wavelength (see Figure 2), whereas the dielectric constants

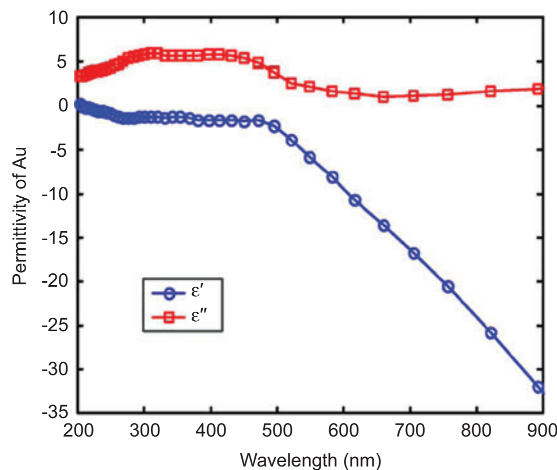

Figure 2 Change of the real and imaginary parts of the complex dielectric constant (permittivity) of gold with the wavelength in the UV, visible, and near-infrared range [33].

of dielectric materials remain nearly unchanged. The polarizability [34] of the plasmon can be described as follows:

$$\alpha=4\pi a^3 (\varepsilon-\varepsilon_m)/(\varepsilon+2\varepsilon_m) \quad (1)$$

where ε_m is the dielectric constant of the surrounding dielectric material and a is the radius of the metallic nanoparticle. The plasmonic polarizability is maximized when the dielectric constant of metal satisfies the following condition:

$$\varepsilon'=-2\varepsilon_m,\ \varepsilon''\rightarrow 0 \quad (2)$$

where ε' and ε'' are the real and imaginary parts of the dielectric constant, respectively.

The aforementioned equation does not include the influence from the nanoscale structure dimension; however, this condition has to be modified when the metallic structure approaches the sub-100-nm scale. At this scale, the dimension of the metallic nanostructure becomes comparable to the mean free path length of the conduction electrons in metal. The physical boundary of the metallic nanostructures poses a boundary condition for the plasmon resonance mode, which is redefined by the following equation [34]:

$$\varepsilon'=-(2+2.4x^2)\varepsilon_m,\ x=2\pi\varepsilon_m^{1/2} a/\lambda \quad (3)$$

where ε' is the real part of the dielectric constant of the metal material, ε_m is the dielectric constant of the surrounding dielectric material, and λ is the optical wavelength. Nanoplasmonic structures are thus referred to the metallic nanostructures with the discrete plasmon resonance modes that are dependent on the nanostructure geometries and surrounding medium.

The response of both SPR and LSPR sensors to change of refractive index can be described by using the following equation [35], which was initially developed for propagating SPR [36]:

$$\Delta\lambda_{max}\approx m\,(n_{adsorbate}-n_{medium})\,[1-\exp(-2d/l_d)] \quad (4)$$

where $\Delta\lambda_{max}$ is the wavelength shift when the reflectance (or SPR) spectrum reaches minimum due to resonant absorption (Figure 1A), m is the sensitivity factor, $n_{adsorbate}$ and n_{medium} are the refractive indices of the adsorbate and medium surrounding the nanoparticle, respectively, d is the effective thickness of the adsorbate layer, and l_d is the electromagnetic field decay length. Therefore, both SPR and LSPR sensors are highly sensitive to the dielectric properties of the medium adjacent to the dielectric-metal interface. Figure 1A shows a typical experimental setup and a resulting reflectance spectrum obtained in an angle-solved mode (measured against angle of incidence at a fixed wavelength) that demonstrates a resonance angle shift upon binding of analyte in a SPR biosensor, whereas Figure 1B illustrates a typical measurement scheme for LSPR biosensors and a resulting scattering spectrum that shows resonance wavelength shift upon binding of DNA (Au-Ph-DNA, red line) to a phosphine (Ph) surfactant coated gold nanoparticle (Au-Ph, green line) [27]. To selectively bind and detect analytes of interest in biosensing, metallic surface of both sensors is generally modified using various strategies such as bioreceptors (Figure 1) and/or hydrophilic coating such as Ph as mentioned above [14, 15].

Brought to you by | University of California - Berkeley (University of California - Berkeley)
Authenticated | 172.16.1.226
Download Date | 7/6/12 12:05 PM

One of the important driving forces in biosensor research is to develop large-scale biosensor arrays composed of highly miniaturized signal transducer elements enabling real-time and parallel monitoring of multiple species, especially for high-throughput screening applications such as drug discovery and proteomics research where many thousands of ligand-receptor or protein-protein interactions must be rapidly measured. To meet this need, LSPR-sensors stand out as better candidates due to the "nano" advantages over SPR [35, 37]. For example, SPR sensors require at minimum a 10×10 μm area for sensing experiments. For LSPR sensors, when delivering the same information as the SPR sensor, the spot size can be minimized down to sub-100-nm regime (around a size of a single nanoparticle) using single nanoparticle LSPR [38, 39]. Moreover, because SPR sensors have the sensitivity factor (*m*) (around 2×10^6 nm/RIU) higher than LSPR sensors do (around 2×10^2 nm/RIU), SPR sensors require accurate control of temperature and complex optical instrumentation, whereas LSPR nanosensors do not. However, the larger sensitivity factor does not mean that SPR sensors are 10,000 times more sensitive than LSPR sensors. As indicated in Eq. (4), the short (and tunable) characteristic EM field decay length (l_d) enhanced the overall sensitivity of the LSPR nanosensors. For example, compared to the 200–300-nm decay length or approximately 15–25% of the light *s* wavelength for the SPR sensors, the decay length of the LSPR sensors can reach approximately 5–15 nm or 1–3% of the light *s* wavelength [38]. Therefore, both are very competitive in their overall sensitivities. However, the overall sensitivity of the LSPR nanosensors depends on many factors and thus varies significantly. Currently, LSPR [17] has not only been recognized as an ultrasensitive method for detecting molecules of both biological and chemical interest but also plays an important role in all other surface-enhanced biosensing techniques such as surface-enhanced Raman scattering (SERS) [19], surface-enhanced hyper-Raman scattering [40], surface-enhanced infrared spectroscopy (SEIRS) [41, 42], and surface-enhanced fluorescence (SEF) [43].

Raman scattering is the inelastic scattering of a photon from a molecule in which the frequency change precisely matches the difference in vibrational energy levels [19]. Raman spectroscopy is a highly specific Raman scattering-based technique that detects and identifies molecules by their unique vibrational fingerprints. However, as a scattering process, the Raman scattering is exceedingly weak: typical Raman scattering cross sections per molecule are in the range of 10^{-30} and 10^{-25} cm^2 [40]. Thus, Raman spectroscopy usually needs a relatively large volume of molecules to produce detectable scattering signal intensities. This disadvantage has prevented Raman spectroscopy from many important sensing applications such as surface and *in vivo* sensing where the number of molecules that produce Raman scattering is small. SERS is about Raman scattering of single molecule or an ensemble of molecules of interest appearing (e.g., by binding and absorbing) in close proximity (within a few nanometers to nanoparticle surface) of a plasmonic nanoparticle that will produce an enhancement of the Raman signal. It was discovered in 1974 [44] and correctly explained in 1977 [45, 46]. Two primary mechanisms are generally thought to be responsible for large SERS signals [19, 26, 40, 47, 48]. First, chemical enhancement (CE) corresponds to any modification of the Raman polarizability tensors (α_R) upon adsorption of the molecule onto the metal surface. It can result from changes in the molecular electronic state or resonant enhancements from either existing molecular excitations or newly formed charge transfer states. Second, both optical excitation and Raman scattering resonate with the LSP modes in the metal nanoparticles (NPs) simultaneously, resulting in local field EM enhancement and radiation EM, respectively [26, 48]. The EM contribution is, in any case, believed to be much larger ($>10^2$) than the CE effect [17]. More specifically [48], if we assume that g is the local field enhancement averaged over the surface of the nanoparticle, the average magnitude of the local field (E_s) around the surface will be: $E_s=g\times E_0$, where E_0 is the magnitude of the incident field. The average molecule on surface will then be excited by the enhanced local field E_s, resulting in the Raman-scattered light near the surface with a field strength $E_R\propto\alpha_R\times E_s\propto\alpha_R\times g\times E_0$. The Raman-scattered (or radiated) fields (E_R) at the Raman-shifted wavelength will be further enhanced by the metal nanoparticle with the radiation enhancement factor g' in the same way as the optical excitation was, giving the magnitude of the SERS-scattered filed $E_{SERS}=\alpha_R\times g'\times E_s\propto\alpha_R\times g'\times g\times E_0$. As the average light intensity is proportional to the square of its electromagnetic field, we will theoretically have the SERS enhancement factor [assuming that the difference in α_R between SERS and non-SERS ($E_{non\text{-}SERS}=\alpha_R\times E_0$) fields can be ignored compared to Ems]:

$$EF=\frac{I_{SERS}}{I_{non-SERS}}=\left(\frac{E_{SERS}}{E_{non-SERS}}\right)^2=g^2.g'^2 \tag{5}$$

Assuming that $g\approx g'$, we will have *EF* the fourth-power dependence on g, the key to the extraordinary enhancements SERS provides. This approximation takes advantage of the fact that the plasmon width is generally large compared to the Stokes shift, especially the low-frequency one. However, for SERS on isolated homogeneous particles where the plasmon width is small, this assumption leads to an overestimate of the EF by factors of 3 or more.

3. Controlled synthesis and nanofabrication of plasmonic nanostructures

The underlying phenomena exploited for nanobiophotonic sensing applications is based on the interaction of light and matter at nanoscale surfaces. When incoming electromagnetic radiation is coupled to localized excitation of conductor electrons at the dielectric-metal interface of a metal nanoparticle, quantitative spectral data as a function of local environmental changes over time can be gathered [49]. Utilizing the plasmon coupling between neighboring geometrical features, the scattering cross-sections of nanostructures should dominate over absorption cross-sections resulting in enhanced scattering spectra of nearby molecular complexes for generation of intense scattered radiation [49]. If the resulting plasmon

Brought to you by | University of California - Berkeley (University of California - Berkeley)
Authenticated | 172.16.1.226
Download Date | 7/6/12 12:05 PM

resonance frequency matches the incoming EM radiation, the collective oscillations of the conduction electrons at the dielectric-metal interface occurs in-phase, and a highly sensitive, label-free, spectral snapshot of the local biochemical environment is obtained. The strong, localized plasmon resonance exhibited by metal nanoparticles is dependent on the surrounding environment as well as composition, size, and shape of the nanoparticle [50]. Sharp features, such as those exhibited by nanostars, can be exploited for "lightning rod effects", where molecules adsorbed to high curvature surfaces show enhanced Raman scattering due to the polarization of metal in those regions resulting from the external EM field [49, 51].

The ability to control the morphology of these "sensing" elements is essential for large-scale LSPR biosensing applications, such as SERS. Recent advances in control over nanoparticle size and shape allow the transfer of plasmon energy as well as electromagnetic energy to be concentrated and transported [50]. Combined with nanostructured surfaces, both *in vitro* and *in vivo* static and dynamic molecular interactions of chemical and biological molecules can be detected [50].

Current LSPR and SERS fabrication methods typically rely on bottom-up nanostructure synthesis, top-down nanostructure fabrication, or combinations of both processes. With bottom-up methods, nanocrystals are synthesized using solution-based chemical or physical processes. The composition, size, and shape of the nanoparticles depend heavily upon control of chemical reactions and conditions during synthesis [16]. Top-down nanostructure fabrication involves lithographic techniques utilizing well-established micro- and nano-fabrication tools. Modified, or hybrid, assembly fabrication may involve combinations of bottom-up and top-down processes, such as nanosphere lithography (NSL), where nanoparticles are used as the masking template for conventional metal deposition techniques and provide another way to obtain sub-micron pattern spacing.

3.1. Bottom-up chemical synthesis

Bottom-up nanostructure synthesis methods include sol-gel, pyrolysis, hydrothermal, micelles, and chemical precipitation from supersaturated conditions [52]. Addition of organic ligands or capping materials can achieve size and shape control of nanoparticles by inhibiting further crystal growth or changing the growth environment to an inert one [52]. Chemical reduction of metal salts with a stabilizer is often used to synthesize metal nanoparticles. The stabilizer functions as a growth inhibitor in particular directions, thus controlling shape as well as providing colloidal stability [16]. A two-step process of metal nanoparticle seeded growth can produce diverse shapes such as rods, plates, and pyramids with high reproducibility [16]. Solution-based synthesis routes typically consist of three stages: first, nucleation; second, transformation of nuclei to seeds; and finally, seed evolution into nanocrystals [53]. Nanoparticle morphology is also controlled by reaction time, temperature, and concentration of solvents, reagents, and surfactants [52]. For seeded growth, the final shape of the metal nanocrystal is determined by the structure of the seed and the capping material binding affinity [53].

Designing nanoparticles using wet chemical processes produces a large variety of shapes and sizes. The simplest form of nanoparticle is the nanosphere, which can be formed from seed-mediated growth, as described earlier [54, 55]. Geometrical shape influences the plasmon resonance response. For solid gold colloidal nanospheres, plasmon resonance typically occurs around 520 nm and can only be tuned around that mode by approximately 50 nm [56]. The shape anisotropy of nanorods can provide additional functionality from two plasmonic resonance modes dependent on the radial and longitudinal axes of the nanorod [50] and tunable by changing the aspect ratio [8]. Other synthesized shapes include cubes, tetrahedrons, octahedrons, triangular plates, bipyramids, and triangular plates [57–59]. Mixed metallic-alloy and shell-core structures have also been demonstrated [56, 60]. Nanoshells, which consist of a spherical dielectric core encased in a metal shell, have tunable plasmonic properties highly sensitive to the inner and outer shell diameters [61], and have the advantage of extending into the near-infrared spectrum, a region of relative transparency for living tissues [62]. Combining the advantages of nanorod shape anisotropy and nanoshells with tunable plasmon resonances results in nanorice, a hybrid nanostructure where plasmon resonance tuning occurs by changing the nanorice length as well as varying the relative size of inner and outer metallic shells [63]. Branched nanoparticles, such as nanostars, are of interest due to their sharp edges and can exhibit higher SERS intensity at the tips [64, 65]. As the LSPR frequency is dependent on both the shape and the size of the nanostructures, the wide variety of NPs mentioned above can have their LSPR frequency varied from the entire visible to mid-infrared part of the EM spectrum as shown in Figure 3, demonstrating the highly tunability of plasmonic nanobiosensors, which enables a wide variety of applications in biomedical detection.

When using nanoparticles for biosensing assay-based applications, the metal or metal-dielectric nanoparticle surfaces are functionalized with biological recognition elements that interact directly with analytes in aqueous solution. Some difficulties associated with functionalizing nanoparticles in aqueous solutions include dependency on pH, temperature, or concentration conditions [16]. Direct placement of nanoparticles on substrates by condensation, deposition, or electrostatic interaction can be applied to avoid the unintentional aggregation of nanoparticles in solution [16]. Top-down fabrication processes and tools, where the nanoscale features are produced directly on the substrate with high repeatability, may provide an alternative to the multistep process of synthesizing nanoparticles by wet chemical means then depositing mono- or bi-layers onto substrates. Additionally, integration with well-established micro- and nanofabrication processes and tools readily provides potential for large-scale manufacturing of LSPR and SERS substrates. Modified, or hybrid, processes often involve a top-down fabrication technique either for pattern transfer or metal deposition and are also discussed in the following section.

Brought to you by | University of California - Berkeley (University of California - Berkeley)
Authenticated | 172.16.1.226
Download Date | 7/6/12 12:05 PM

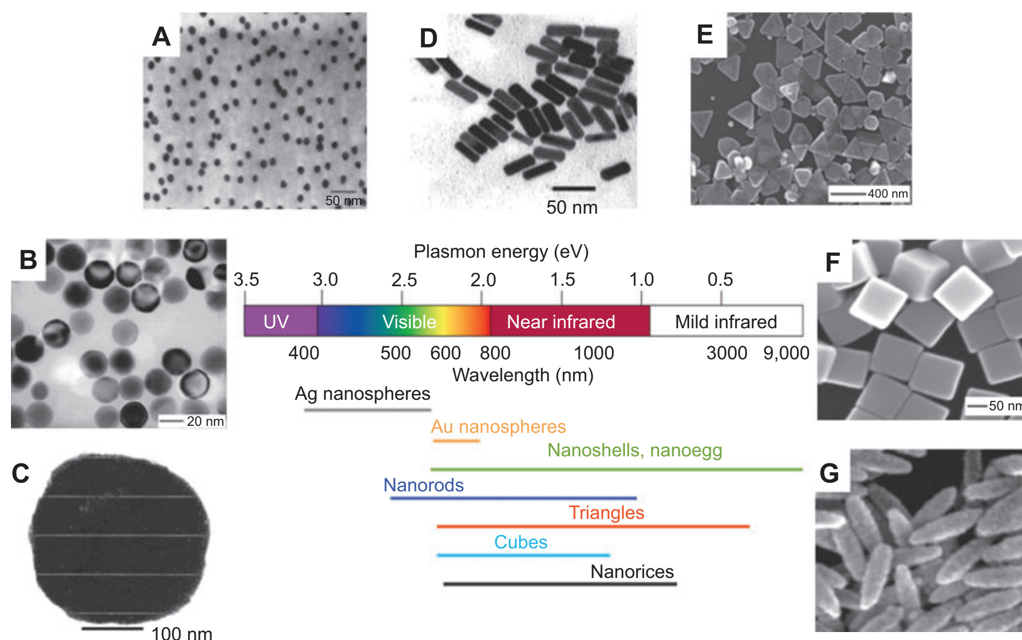

Figure 3 Nanoparticle resonance range of plasmon resonances for a variety of particle morphologies [3]. TEM images of Au spheres (A) [54], Ag spheres (B) [55], SiO_2/Ag (core/shell) nanoshells (C), and nanorods (D) [66]; SEM images of cubes (F) [58], nanorices (G) [63], and triangular plates (E) [59].

3.2. Top-down nanofabrication

In addition to utilizing existing and well-established nanofabrication tools, top-down fabrication of LSPR and SERS substrates can also provide reproducible control over feature size, shape, and gap distance between nanostructures. The typical process involves two steps. First, nanoscale pattern transfer to a substrate must occur with one of the major lithographic techniques, which include electron-beam (EBL), nanoimprint (NIL), template (such as anodic aluminum oxide, AAO), and nanosphere (NSL). The second process can involve metal deposition onto the substrate using vapor deposition via chemical (CVD), physical (PVD), oblique-angle (OAD), or glancing-angle (GLAD) methods, or an etching process. Focused ion beam (FIB) milling is another technique to create nanoscale features, although unintended doping of substrates with gallium ions can modify optical properties, especially in the visible light region [67, 68]. Additional techniques to form metal nanostructures include laser ablation of metal targets in aqueous solution and electrodeposition, although the latter process is limited to metallic substrates [69]. Table 1 compares current top-down fabrication techniques, using SERS substrates as examples for nanoplasmonic biosensors. Typically, the molecule used for SERS experiments exhibit a large Raman scattering cross-section.

3.2.1. Electron-beam lithography (EBL) EBL is a direct-write nanopattern transfer method using a virtual mask for sequential feature exposure on a substrate. High-resolution features down to 10 nm are obtainable [85]. Advantages of EBL include nanoscale feature resolution, control over beam energy and dose, elimination of physical masks, high accuracy over small regions on a wafer, reduction in defect densities, and ability for large depth of focus on changing topographies [85]. Although EBL provides an effective method for fabricating reproducible nanoscale features including nanodots [67], nanowells [86], and nanoring antennas [87], the longer writing times and higher costs are the main disadvantages of using EBL for high-throughput, low-cost LSPR and SERS applications.

3.2.2. Nanoimprint lithography (NIL) A potential low-cost, large-scale method for SERS substrate fabrication is NIL. The process is twofold: a hard mask, typically made of metal, dielectrics or semiconductor material, is pressed into a thin layer of polymer heated above its glass transition temperature [88]. When pressed together, the viscous polymer conforms to the mold topography, creating thickness variations in the substrate upon removal of the mold [89]. A reactive ion etch (RIE) of the substrate completes the pattern transfer. NIL processes have been used to create gold rectangular, cylindrical, and diamond-shaped nanoblocks based on grating mold orientation [90], flat, grated, and pillared silver nanostructures for SERS [91], and gold nanodisks [92]. A potential disadvantage of the NIL process is the embedded cost of fabricating the original mold, which requires access to high-resolution lithographic tools, such as EBL. The mold-making process involves placing resist on the mold substrate, nanopattern exposure, hard mask (metal) deposition on the template, followed by liftoff and RIE for selective etching of the mold [93]. Once the NIL mold is fabricated, multiple transfers provide a high level of repeatability for nanoscale features.

Brought to you by | University of California - Berkeley (University of California - Berkeley)
Authenticated | 172.16.1.226
Download Date | 7/6/12 12:05 PM

Table 1 Comparison of various top-down nanofabrication techniques for SERS substrates.

	EF[a]	Typical substrate area /cm^2	Uniformity	Reproducibility	Material/shape[b]/size/nm[c]	Molecule/laser wavelength/nm	Cost
EBL	10^5 for BSA, 10^7 RNase-A [70]	<0.001×0.001 [71]	–	<20% [72]	Ag or Au/film on pillars/25 nm [72]	Rhodamine 6G (R6G) and 1,10-phenanthroline[72]/632.8 nm Bovine serum albumin (BSA) and ribonuclease-A (RNase-A) [70]/632.8 nm	Expensive
NSL	10^8 [73–75]	1.5×1.5 [76]	–	–	5–40 nm [77]	Benzenethiol (BT) [75]	Inexpensive
Template	10^6 [78]	1×0.5 [79]	<20% [79]	<15% [79]	Au/NP/110 [79]	Thionine [79]	Inexpensive
Hybrid [80]	10^5	1×1	–	–	50 nm thick Ag	BT	Inexpensive
OAD	10^6–10^8 [81] >10^8 [82]	2.5×7.5 [81]	<10% [81]	<15% [81]	Ag/NR/ ~88–99 [81]/ 80–90 [82]	Trans-1,2-bix(4-pyridyl)ethane (BPE) /785 [82]	Moderate
GLAD	–	–	–	–	Ag/NR/20–30 [83]	R6G	Moderate
AAO/GLAD [84]	10^5	–	–	–	Pt, Au, ITO/NT/ 20–200 nm	Benzenethiolate	Moderate

[a] Enhancement factor.
[b] Minimum dimension of nanostructure.
[c] NP, nanopillar; NR, nanorod; NT, nanotube.

3.2.3. Template-based methods Template-based methods typically utilize the regular array of nanometer scale holes in a hard material such as AAO for electrochemical deposition of metals, semiconductors, or polymers [78, 94]. For AAO templates, the pore diameter is controlled by changes in oxidation conditions and feature sizes can range from 5 to 500 nm [95]. Following material deposition, which can include electrochemical, thermal vacuum evaporation, or radio frequency (RF) sputtering, the AAO template is removed by chemical dissolution [95, 96]. The advantages of AAO templates include large working areas (>1 cm^2), compatibility with different materials, and tunable size properties [95]. AAO-templated nanostructures for plasmonic applications include nanorods [96, 97], nanopores [98], nanopillars [79], nanowires [78], and nanocrescents [99]. Depending on the composition of the electrochemical solution, surface roughness and different lengths of resulting nanostructures may result [97]. Branching of nanostructures at the base is also another issue with the process and pore diameters of <20 nm can exhibit irregular patterns [95, 96]. As shown in Table 1, SERS enhancement factors up to 10^5 have been demonstrated with a hybrid AAO template and glancing angle deposition technique [84]. Block copolymers (BCPs) are another technique to fabricate template-based nanostructures for LSPR applications. Nanostructure shapes such as spheres, cylinders, and lamellae are all dependent on the composition and chain structure of the polymers [100], with feature sizes ranging from 5 to 50 nm as a function of the BCP molecular weights and final self-assembled nanoparticle pattern dependent upon the BCP domain symmetry. Although micrometer scale areas are achievable, defects can exist at grain boundary edges [101]. Using a combination of top-down and bottom-up processes, examples of defect-free, large area BCP domains on templated and lithographically defined surfaces have been demonstrated [101, 102]. The high cost of extreme ultraviolet interferometric lithography limits wide-scale application of the latter process [101], whereas EBL grooves combined with plasma etching is required for the former [102].

3.2.4. Nanosphere lithography (NSL) NSL is based on templating monolayer or double layer colloidal nanoparticles for submicron and nanometer scale patterns. Methods for preparing NSL include electrostatic deposition, self-assembly, drop casting, spin coating, and evaporation [95, 103] forming a hexagonal, close-packed monolayer on the substrate with controllable size, shape and interparticle spacing [104]. Metal is deposited onto the nanoparticle array by thermal, e-beam or pulsed laser deposition, and then the NSL templates are removed from the substrate at high temperatures or with chemical dissolution using organic solvents [95]. NSL advantages include low-cost, high-throughput, compatibility with many materials, and the capability of producing well-ordered arrays on different substrates [105]. Nanostructures such as nanopillars [106], nanohole arrays [107], nanowire arrays [108], nanobowls [109], nanotriangles [104], nanorings [110], and nanocrescents [49] have been fabricated successfully for LSPR and SERS applications. However, NSL has several disadvantages. First, formation of colloidal

Brought to you by | University of California - Berkeley (University of California - Berkeley)
Authenticated | 172.16.1.226
Download Date | 7/6/12 12:05 PM

particles into a mask has limited geometries due to the hexagonal close packed formation [111]. Modified NSL with varying gaps can be fabricated, involving multiple processes such as etching, ion beam techniques, or spin coating prior to pattern transfer [111, 112]. As gap sizes affect the tunability of substrate plasmonic resonances [113], it is important to have flexibility with adjusting the gap between particles. Because the size of nanoparticles and gap distance between holes or features are interdependent, control over substrate features has additional constraints [111]. Finally, structural defects such as nanosphere polydispersity, dislocations, vacancies, polycrystalline domains, or local polystyrene (PS), or latex bead disorder are often transferred to the new substrates leaving limited defect-free areas ranging from 10 to 100 μm^2 [77, 114]. The NSL method has been modified in multiple ways, including transferring monolayers via submersion in water [115], liquid/gas interface self-assembly [77], angle-resolved NSL [76], shadow NSL with annealed PS, and fabricating dimers [16]. For SERS applications, Ag film over nanosphere substrates (AgFON) has shown a 10–100× increase in enhancement factor [107].

3.2.5. Oblique angle deposition (OAD) and glancing angle deposition (GLAD) OAD combines physical vapor deposition, such as electron-beam deposition, with steep substrate angles >75° relative to the vapor source. Thin films produced by PVD tend to have columnar or porous microstructures and tilting the substrate at steep angles (>75°) relative to the substrate normal leads to geometrical shadowing effects and preferential growth of nanostructures [116]. As shown in Figure 4A, atoms condense and diffuse on the substrate surface then form nuclei. The region behind the nuclei does not receive additional vapor due to line-of-sight self-shadowing so that incoming atoms deposit on the exposed face of the nuclei [118]. Columns then grow from the nuclei at an angle dependent on the incoming vapor flux direction (Figure 4A). Figure 4C shows the OAD shadowing effect on a lithographically patterned seed layer. Materials used for OAD include metals, metal oxides, silicon, silicon oxides, as well as combinations [117] and SERS enhancement factors have been demonstrated as high as 10^8 (Table 1).

When combined with precision motor control, OAD becomes GLAD, a method for sculpting thin films. Figure 4B shows a typical GLAD apparatus [119]. The design of nanostructures depends on both substrate angle relative to the vapor source and control over the substrate, often accomplished with stepper motors controlling α and ϕ rotational speeds. As shown in Figure 5A, fabricated morphologies range from close-packed nanospheres and tilted nanowires to chevrons, helical posts [117], and nanotubes [124]. Silicon nanowires can be used as templates for high aspect ratio hollow nanostructures [124]. In this case, the tube wall thickness is dependent on the reaction rate and duration of LPCVD coating and crystallinity is a function of the temperature or a post-process anneal [124]. More complicated structures such as helical columns and zigzag nanotube arrays, and square spiral structures have also been demonstrated [124–126]. As shown in Table 1, Ag nanorods were fabricated and tested using R6G, although the enhancement factor was not calculated because 10^{-14} mol/l was the detection limit for the

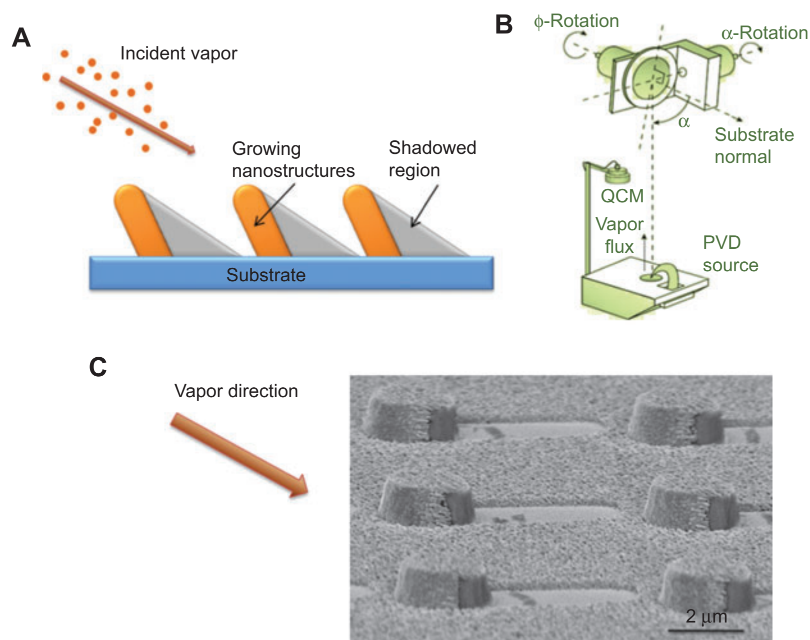

Figure 4 Schematic of oblique angle deposition (OAD) or glancing angle deposition (GLAD). (A) Conceptual illustration of column growth. (B) A typical GLAD apparatus that consists of a rotation stage with substrate angle adjustment [117]. (C) Example of shadowing effect with lithographically patterned substrate.

Brought to you by | University of California - Berkeley (University of California - Berkeley)
Authenticated | 172.16.1.226
Download Date | 7/6/12 12:05 PM

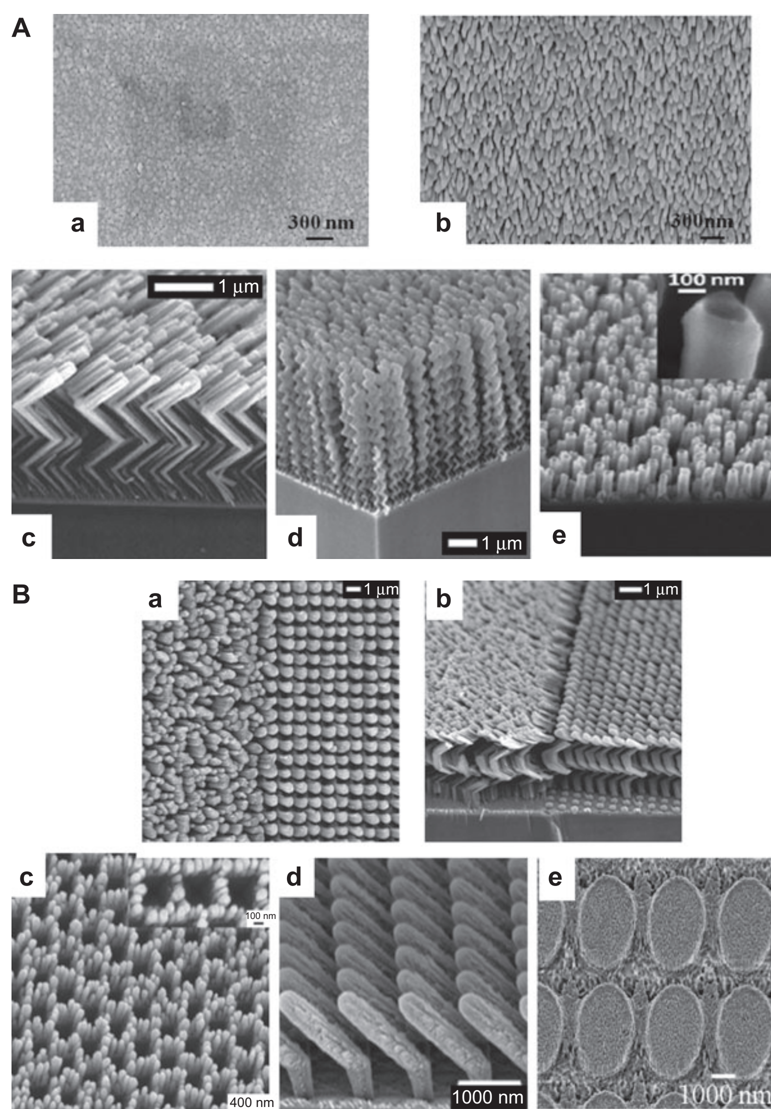

Figure 5 Various morphologies fabricated by GLAD. (A) Various non-patterned morphologies: Ag spheres (a) and tilt nanowires (b), Si chevrons (c) and helical posts (d) [117], and nanotubes (e) [120]. (B) Various patterned nanostructures fabricated by combining GLAD with e-beam lithography (a, b) [121, 117], nanosphere lithography (c) [122], and photolithography (d) [123] and (e).

particular substrate. Although GLAD techniques show promise for further morphology control of substrates, further optimization is required to better control spacing, size, and shape of nanostructures [83].

Although traditional GLAD and OAD processes yield randomized nanostructure formation which in turn produces rods of varying lengths [82], periodic arrays of lithographically patterned seed areas can restrict growth to specific regions by taking advantage of the self-shadowing effect [126]. Conventional micro- or nanofabrication tools can be used to pattern desired seed topography. These seeds then define the initial stages of film growth by removing the randomness of nucleation sites [117]. Successful seed patterning depends on several parameters: first, the seed diameter should be of similar diameter as an individual column to avoid multiple columns growing per seed; second, column broadening can be avoided by designing the relative density of the GLAD film close to the portion of the substrate area covered by patterned seeds; finally, column formation between seeds can be prevented by careful placement of the seed shadow [119]. Seed dimensions are typically several hundred nanometers for inorganic materials with intervals of 100 nm to 1 μm and require large patterned areas (~several mm^2) [117]. Figure 5B shows examples of patterned seed layers and resulting GLAD nanostructure formation. GLAD techniques can also be used to fabricate hetero-nanostructures including gold-coated silicon “matchsticks” for biosensing applications [127] and gold-titanium dioxide-gold sandwich structures for LSPR substrates [121]. For OAD seed patterned silver nanorods, SERS intensities were also shown to increase as both diameter and rod spacing decreased [128], indicating that morphology control may help improve SERS detection.

Brought to you by | University of California - Berkeley (University of California - Berkeley)
Authenticated | 172.16.1.226
Download Date | 7/6/12 12:05 PM

4. Surface biofunctionalization of plasmonic nanomaterials

The significant advancement in controlled nanofabrication offers researchers the capability to tune plasmonic properties of nanomaterials. However, the surface of plasmonic nanomaterials (gold and silver NPs are most common) cannot interact with the biological analyte selectively. To overcome this limit, surface functionalization techniques of nanomaterials by biological recognition elements (bio-receptors or bio-probes) have recently been developed to form hybrid nanomaterials that incorporate the highly selective catalytic and recognition properties of biomaterials such as enzymes and DNA, with the highly sensitive and easily tunable electronic and photonic features of plasmonic nanomaterials [13, 15, 129].

Often, NPs synthesized in organic medium tend to aggregate to form clusters in an aqueous solution that is generally required by biomedical applications. Therefore, before they can be modified by any bioreceptors, water solubilization is required, during which colloidally unstable NPs are stabilized in an aqueous solution by conjugating with hydrophilic ligands. One way to stabilize NPs is by coulombic repulsion. It requires the ligands to be ionic. Another way to stabilize NPs is steric stabilization, during which NP aggregation is prevented by coating with a physical barrier. The barriers include polymeric ligands, such as poly (ethylene glycol) (PEG) [130] and small-molecular ligands such as bis(p-sulfonatophenyl) phenylphosphine surfactants [27]. All these ligands for water solubilization are then replaced by phase transfer or ligand exchange or modified by ligand addition with desired biofunctional ligands [13]. Water solubilization may be performed either as the final stage of the biofunctionalization process of NPs or as an intermediate stage.

Four strategies are generally used to functionalize the surface of plasmonic nanomaterials (typically Au, Ag, and Cu surface) with biomolecules such as bioreceptors. The first is electrostatic adsorption of positively charged biomolecules to negatively charged nanoparticles or vice versa. For example, gold and silver NPs synthesized by citrate reduction are stabilized by citrate ligands at pH slightly above their isoelectric point, resulting in the anionic citrate coated NPs that can be bound to the positively charged amino acid side chains of immunoglobulin G (IgG) molecules [131]. The second strategy is ligand-like binding to metallic surface of plasmonic nanomaterials by chemisorption of, e.g., thiol groups. Metal nanostructures can be functionalized with L-cysteine through the Au-S bonds and then bound to target proteins through peptide bonds with the cysteine moieties [132]. They can also be directly bound to thiol derivative analytes such as protein containing cysteine residues (e.g., serum albumin) [133] or thiolated DNA [134, 135]. The third strategy is covalent binding through bifunctional linkers, exploiting functional groups on both particles and biomolecules. The bifunctional linkers have anchor groups that can be attached to NP surfaces and functional groups that can be further covalently coupled to the target biomolecules. They are extensively used to covalently conjugate biomolecules with various NPs [136], especially when no linking moieties such as thiol groups are available in biomolecules. The common anchor groups include thiols, disulfides, and phosphine ligands that are used to bind the bifunctional linkers to Au, Ag, CdS, and CdSe NPs. The fourth strategy is based on non-covalent, affinity-based receptor-ligand systems. More specifically, nanoparticles are functionalized with bioreceptors (e.g., antibodies) that provide affinity sites for binding of the corresponding ligand (e.g., antigens) or ligand-modified proteins and oligonucleotides. The most well known example in the past several decades is the avidin-biotin system [137, 138]. For example, biotinylated proteins (e.g., immunoglobulins and serum albumins) or biotinylated oligonucleotides (e.g., single-stranded DNA, ssDNA) [135] have been widely used to modify streptavidin-functionalized Au NPs by affinity binding [136]. Regarding molecular recognition, the system consists of the small molecule biotin (vitamin H) as ligand, and the globular protein avidin that is present, e.g., in egg whites as a receptor. Avidin consists of four identical subunits, yielding four binding pockets that specifically recognize and bind to biotin. The dissociation constant is of the order of 10^{15} M and the affinity bond, although not covalent, is found to be extremely stable, resisting harsh chemical and physical (e.g., elevated temperature) conditions.

5. Applications

The strong optical response of plasmonic nanostructures due to LSPR is also critical to many biomedical applications. The different optical responses that result from this phenomenon and the corresponding applications are shown in Figure 6. Light scattering is used primarily in imaging techniques such as optical coherence tomography (OCT) where the presence of particles with large scattering cross-sections enhances image contrast, and dark-field microscopy, where transmitted light is blocked and scattered light is collected, showing scattering particles with a bright color against a dark background. Absorption is used in a variety of techniques that take advantage of the fact that strongly absorbing plasmonic nanostructures can become highly localized heat sources when irradiated with a laser through the photothermal effect. The generated heat can be used to initiate release in drug delivery systems, enhance contrast in optical imaging techniques such as photoacoustic imaging, and provide photothermal treatment. Examples for some of those techniques will be described in more detail in the following sections.

5.1. Case 1: molecular plasmonic rulers

Förster resonance energy transfer (FRET) has served as a molecular ruler to monitor conformational changes and measure intramolecular distances of single biomolecules [139–141]. However, such a ruler can suffer from difficulty in distinguishing changes in relative dye orientation from changes in distance [139], limited observation time of a few tens of seconds due to blinking and rapid photobleaching of fluorescence, and an upper distance limit of ~10 nm.

Brought to you by | University of California - Berkeley (University of California - Berkeley)
Authenticated | 172.16.1.226
Download Date | 7/6/12 12:05 PM

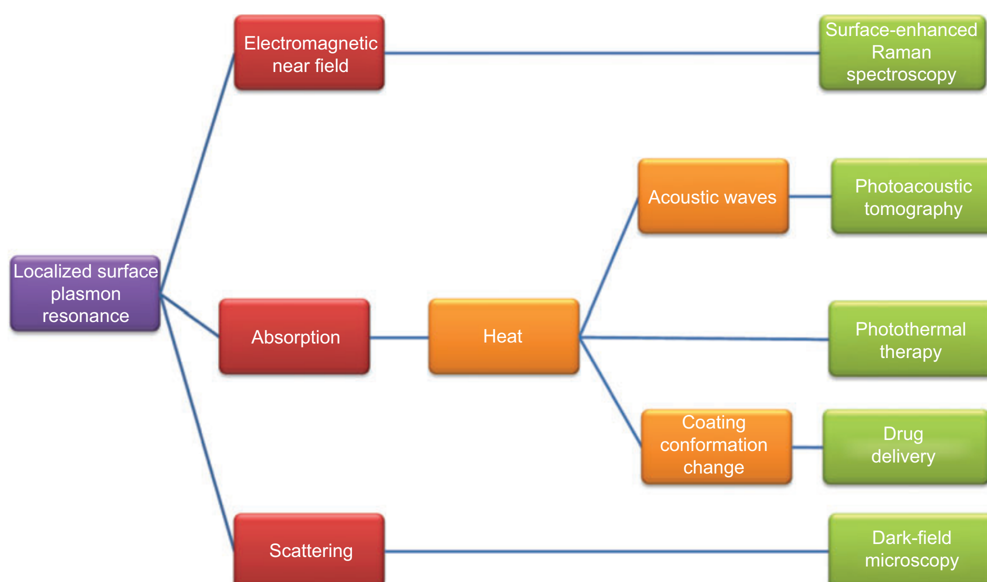

Figure 6 Localized surface plasmon resonance (LSPR) is the origin of a number of interesting phenomena observed with plasmonic nanostructures.

Silver and gold NPs have LSPR in the visible range and do not blink or bleach. Sonnichsen et al. have exploited LSPR wavelength shifts as a new class of molecular ruler to monitor distance between ssDNA linked single pairs of Au, Ag NPs or both [135], overcoming the limitations of organic fluorophores [142, 143]. They first attached a streptavidin functionalized NP to the bovine serum albumin (BSA)-biotin coated glass surface and then introduced a second NP modified by thiol-ssDNA-biotin bifunctional linker to be attached to the first NP via biotin/streptavidin binding (Figure 7A, C). Light scattering was measured by transmission dark field microscopes (Figure 7A). For both gold and silver NPs, they observed the significant color change and spectral shift between a single isolated NP and a pair of adjacent NPs (Figure 7B–E). The LSPR shift was used to follow the directed assembly of gold and silver nanoparticle dimer in real time. The team also used the ruler to study the kinetics of single DNA hybridization events by monitoring the LSPR shift (Figure 7F) due to the resulting 2-nm distance increase between the pair of the adjacent NP. These "plasmon rulers" make it possible to continuously monitor separations of up to 70 nm for >3000 s and become an alternative to dye based FRET for *in vitro* single-molecule experiments, especially for applications demanding long observation times without dye bleaching.

Liu et al. demonstrate another molecular ruler in which double-stranded DNA (dsDNA) is attached to a 40-nm Au nanoparticle through the thiol-Au chemistry [27]. Instead of monitoring the LSPR between a pair of DNA linked metal NPs, they monitor the LSPR of individual Au-DNA conjugates cleaved by various endonuclease enzymes. The team found that the LSPR λ_{max} increases with the increased length of the attached dsDNA (Figure 8). An average λ_{max} red-shift of approximately 1.24 nm is observed per DNA base pair. They also used this nanoplasmonic molecular ruler to monitor, in real time, DNA being digested by an enzyme. Therefore, this system allows for a label-free, quantitative, real-time measurement of nuclease activity with a time resolution of one second due to high quantum efficiency of Rayleigh scattering compared with fluorescence or Raman scattering. They can also serve as a new DNA footprinting platform that can accurately detect and map the specific binding of a protein to DNA, which is essential to genetic information processing.

5.2. Case 2: plasmonic Fano resonance protein sensor

Another type of plasmonic resonance sensor is a nanoresonance device which shows both light and dark plasmon resonance mode [144]. Yanik et al. introduced an ultrasensitive label-free detection technique based on asymmetric Fano resonances in plasmonic nanoholes (Figures 9 and 10) [145]. To fabricate high-quality sensors, they used a lift-off free evaporation fabrication technique with uniform and precisely controlled nanofeatures over large areas with resonance line-widths comparable to that of the simulated structures (Figure 9). By exploiting extraordinary light transmission phenomena through high-quality factor (~200) subradiant dark modes in the nanoholes, they experimentally demonstrated high sensitivity for intrinsic detection limits surpassing that of conventional surface-plasmon sensors. The high sensitivities are attributed to the suppression of the radiative losses owing to the sub-radiant nature of the Fano resonances which exhibit dramatic intensity changes to small perturbations within their local environment. The researchers show direct detection of a single monolayer of biomolecules with the naked eye using the plasmonic Fano resonance sensor by eliminating the need for fluorescent labeling and optical detection instrumentation.

Brought to you by | University of California - Berkeley (University of California - Berkeley)
Authenticated | 172.16.1.226
Download Date | 7/6/12 12:05 PM

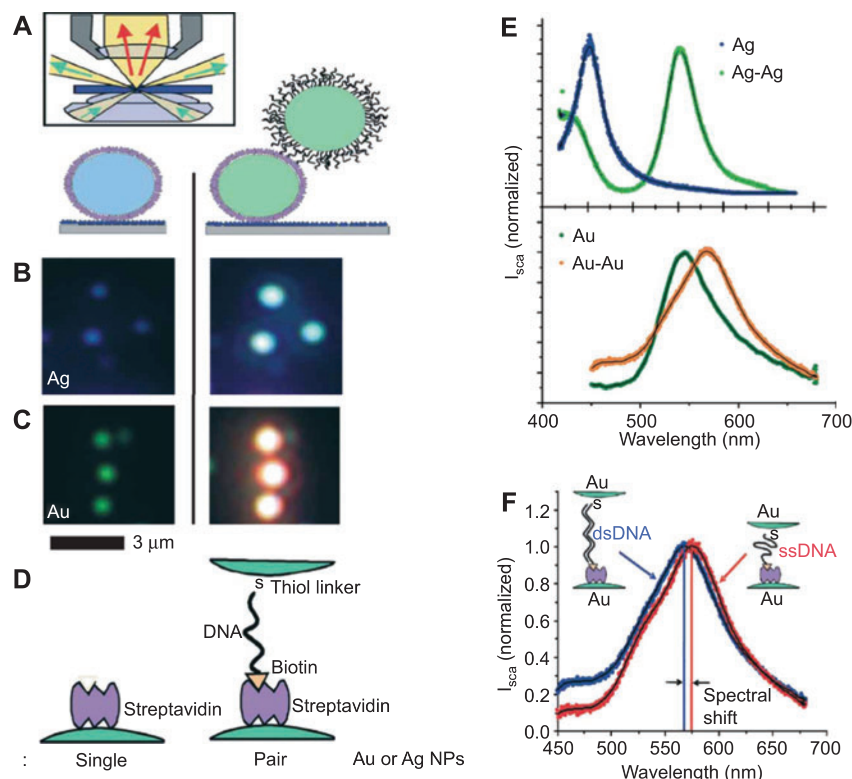

Figure 7 DNA-functionalized gold and silver nanoparticles (NPs) as molecular plasmonic rulers [135]. (A) First, streptavidin functionalized nanoparticles are attached to the BSA-biotin coated glass surface (a, d left). Then, a second NP is modified by thiol-ssDNA-biotin bifunctional linker and then attached to the first particle via biotin-streptavidin affinity binding (a, d right). Inset: principle of transmission dark field microscopy. (B) Single silver particles appear blue (left) and particle pairs appear blue-green (right). (C) Single gold particles appear green (left) and gold particle pairs appear orange (right). (E) Representative scattering spectra of single particles and particle pairs for silver (top) and gold (bottom). The LSPR scattering spectrum for silver NPs shows a larger LSPR shift (102 nm vs. 23 nm), stronger light scattering, and a smaller half width at half maxima (HWHM) than gold particles. (F) Example of the LSPR spectral shift between a gold particle pair connected with ssDNA (red) and dsDNA (blue), corresponding to the distance increase of 2.1 nm between the particle pair upon DNA hybridization.

5.3. Case 3: coupling LSPR with SERS

For a particular Raman band, Van Duyne and his team found that the optimal condition is achieved when the LSPR λ_{max} equals the excitation wavelength (in absolute wavenumbers) minus one-half the Stokes shift of the Raman scattering band [75]. Furthermore, the LSPR can be easily tuned by changing the size and shape of NPs. Therefore, LSPR nanobiosensors become ideal candidates for a complementary molecular identification platform to SERS [17] so that Raman fingerprint could be used to identify unknown molecules that cannot be achieved by biological recognition elements of LSPR nanobiosensors. The team demonstrated the complementary nature of LSPR spectral-shift assays and SERS molecular identification with the anti-dinitrophenyl immunoassay system [146]. Binding of the anti-dinitrophenyl ligand to 2,4-dinitrobenzoic acid was quantified by measuring LSPR shift, whereas SERS was used to verify the identity of the adsorbed molecules.

Notably, Coppe et al. present a unique solid surface of high-aspect-ratio silver-coated silicon nanocone arrays that allows highly uniform molecular deposition and thus subsequent uniform optical imaging and spectroscopic molecular detection without any surface chemistry modification (Figures 11 and 12) [147]. Both dye molecules and unlabeled oligo or peptides are printed on the metallic nanocone photonic substrate surface as circular spot arrays. In comparison with the printed results on ordinary glass slides and silver-coated glass slides, not only high-printing density but also uniform molecular distribution in every deposited spot is achieved. The high-uniformity and repeatability of molecular depositions on the "coffee stain"-free nanocone surface is confirmed by laser scanning fluorescence imaging and SERS imaging experiments. The physical mechanism for the uniform molecular deposition is attributed to the super hydrophobicity and localized pinned liquid-solid-air interface on the silver-coated silicon nanocone surface. The unique surface properties of the presented nanocone surface enabled high-density, high-uniformity probe spotting beneficial for genomic and proteomic microarrays and surface molecular imaging.

5.4. Case 4: silver-enhanced arrays

Taton et al. significantly improved the selectivity and sensitivity of arrayed detection of nucleic acids by silver-coated gold nanoparticles (GNPs) (Figure 13) [142], comparing to the analogous fluorophores system. Nucleic acid target sequences

Brought to you by | University of California - Berkeley (University of California - Berkeley)
Authenticated | 172.16.1.226
Download Date | 7/6/12 12:05 PM

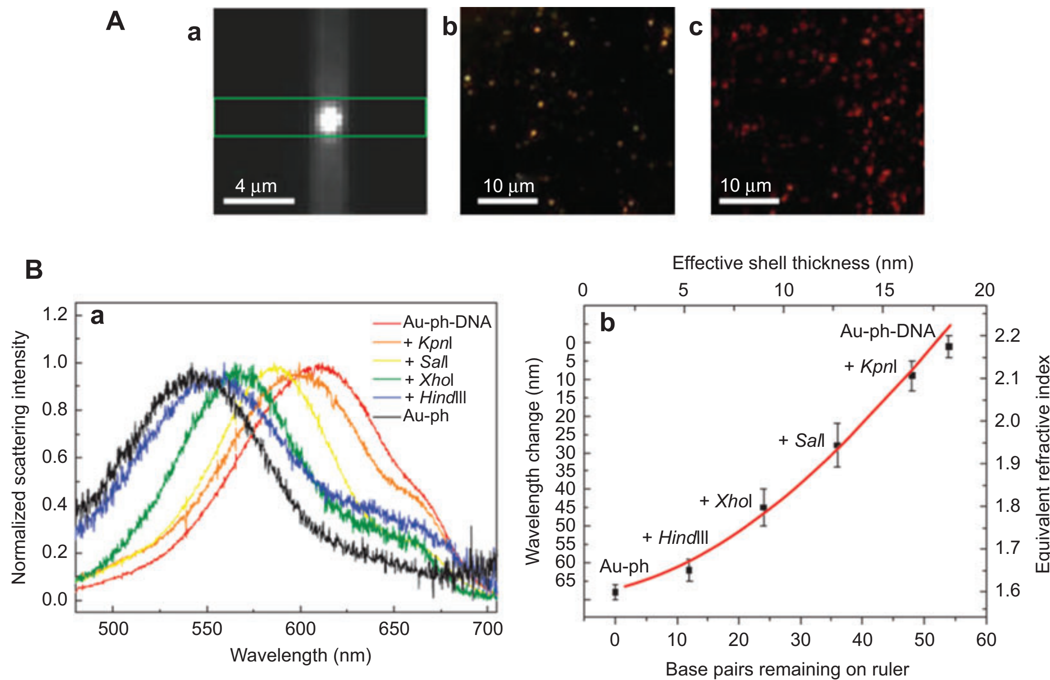

Figure 8 Nanoplasmonic molecular rulers for measuring nuclease activity [27]. (A) Dark field scattering images: a, single target single nanoparticle isolated from other Au or Au-DNA NPs for spectroscopic examination; b, c, true-color images of single Au NP (b) (540 nm peak) and Au-DNA NP (c) (607 nm peak). (B) Typical LSPR scattering spectra (a) of the Au-DNA nanoconjugates after cleavage reactions with four endonucleases (*Hind*III, *Xho*I, *Sal*I, and *Kpn*I) and the corresponding shift of maximum scattering wavelengths (λ_{max}) (b) as a function of the number of base pairs remaining attached to the Au nanoparticle after the cleavage. The red curve is a fit from a semi-empirical model using a Langevin-type dependence of the refractive index versus dsDNA length. The error bars represent the standard deviation in the measurement of 20 nanoparticles.

were sandwiched between oligonucleotides functionalized GNPs and an array of allele-specific capture probes covalently bound to a glass substrate. After the enhancement by developed silver coating, the arrays (spot size after enhancement is 200 μm) were imaged with an ordinary document scanner (600 dots per inch) and analyzed with standard imaging software (Adobe Photoshop, Adobe Systems Incorporated, San Jose, CA, USA). Sensitivity was greater than the one when a fluorescent dye was used as the label by two orders of magnitudes. When hybridization was carried out at the highest temperature of 50°C, selectivity for perfectly matched sequences over single base mismatches was improved over three times. More recently, the sensitivity of this approach has been further improved at Nanosphere, Inc. (Northbrook, IL, USA) by automating the silver enhancement with an imaging system in which evanescent light is generated by total internal reflection and scattered by the silver-coated GNPs. The scattered light was detected by a CCD camera [148–150]. In this way, unamplified DNA and RNA target sequences became detectable in the presence of genomic DNA. In a typical genotyping assay, genomic DNA is

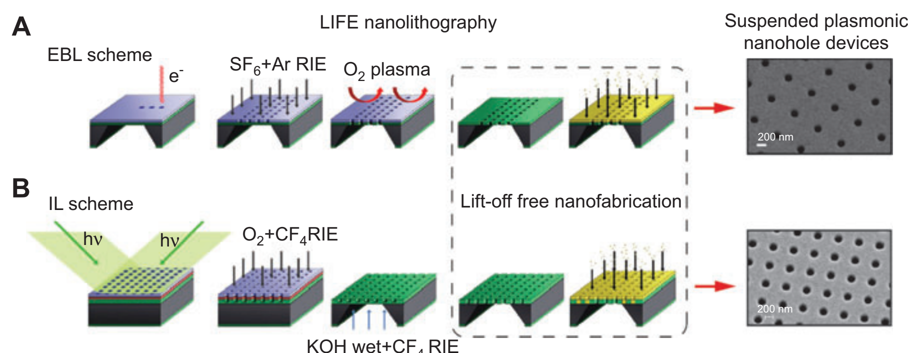

Figure 9 Lift-off free evaporation (LIFE) nanolithography is summarized for schemes based on (A) electron-beam and (B) interference lithography. SEM images of the fabricated devices are shown for (A) p=600 nm, d=180 nm and (B) p=580 nm and d=230 nm, where p is the lattice periodicity and d is the nanohole diameter [145].

Brought to you by | University of California - Berkeley (University of California - Berkeley)
Authenticated | 172.16.1.226
Download Date | 7/6/12 12:05 PM

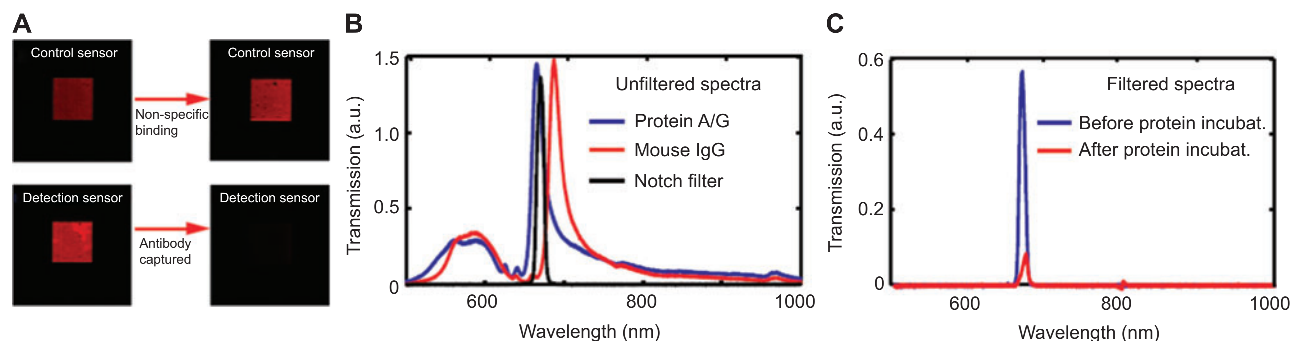

Figure 10 Extremely sharp plasmonic Fano resonances in high-quality nanohole sensors enable seeing single biomolecular monolayers with the naked eye. (A) CCD images of the transmitted light obtained from detection and control sensors are compared. Capturing of the antibody causes a dramatic reduction of the transmitted light intensities through the detection sensors. (B) Transmission spectra are shown before (blue curve) and after (red curve) the capturing of the antibody. Spectral characteristic of the notch filter is also given (green curve). (C) Transmitted light intensities in the presence of the notch filter is given before (blue curve) and after (red curve) the capturing of the antibody [145].

fragmented (size: 300–500 base) and hybridized to a microarray premodified by allele-specific capture oligonucleotides. Those fragments were then labeled with oligonucleotides modified GNPs. After washing away unbound GNPs, SPP modes of the silver-shell coated GNPs are coupled with the evanescent field induced by total internal reflection of either white light or light from LEDs (λ_{max} : 630 nm). The resulting enhanced scattering light, the signal, is quantified with a proprietary reader

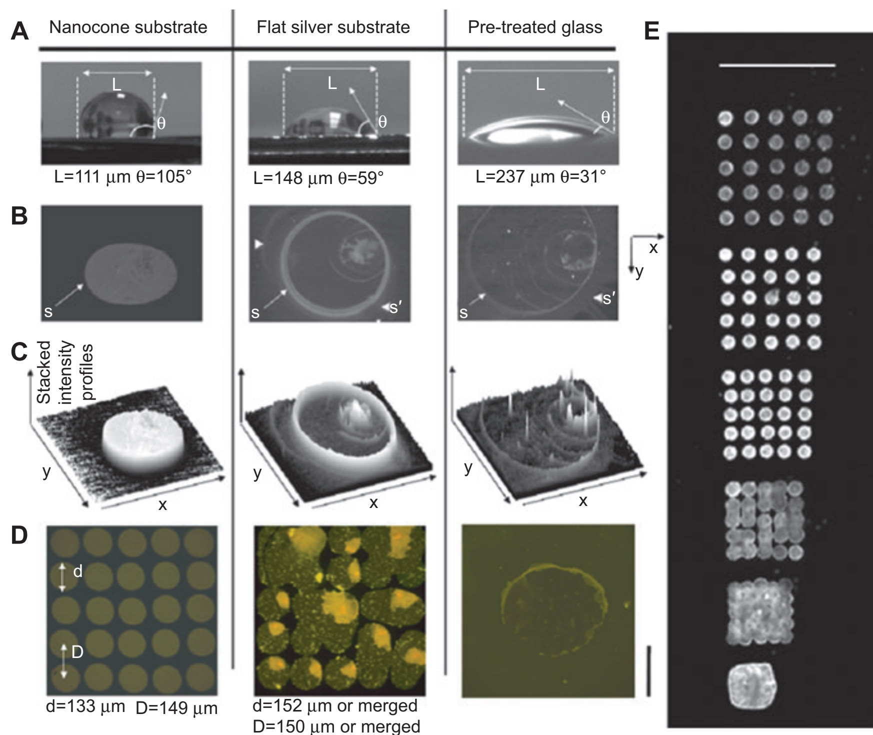

Figure 11 Liquid droplets and molecule depositions on various substrate surfaces [147]. (A) Side view images of liquid droplets dispensed on the silver-coated nanocone substrate, flat silver surface, and pretreated glass slide, respectively from left to right. The diameter (*D*) and contact angles (*θ*) of the liquid droplets are annotated. The water droplet contains 100 µm Rhodamine 6G (R6G) molecules. (B) Laser scanning fluorescence images of R6G molecules deposited on the above three types of substrate surfaces after the droplets dried. The boundaries of the main molecule deposition patterns are denoted by S and those of the peripheral deposition are denoted by S′. (C) A three-dimensional (3D) image representation to evaluate optical homogeneity of molecule deposition. Intensity profiles from two-dimensional (2D) images in (B) are converted to a 3D surface plot in which the height represents the fluorescence intensity or molecule density. (D) Fluorescence images of a 5×5 array of molecule deposition spots. Dimensions of deposition [spot center-to-center (*D*) and diameter (*d*)] are measured and annotated. The scale bar on the right represents 200 µm. (E) Array printing images on the silver-coated nanocone substrate with the spacing between spots of 200, 150, 100, and 50 µm from top to bottom. The scale bar on the top represents 1 mm distance.

Brought to you by | University of California - Berkeley (University of California - Berkeley)
Authenticated | 172.16.1.226
Download Date | 7/6/12 12:05 PM

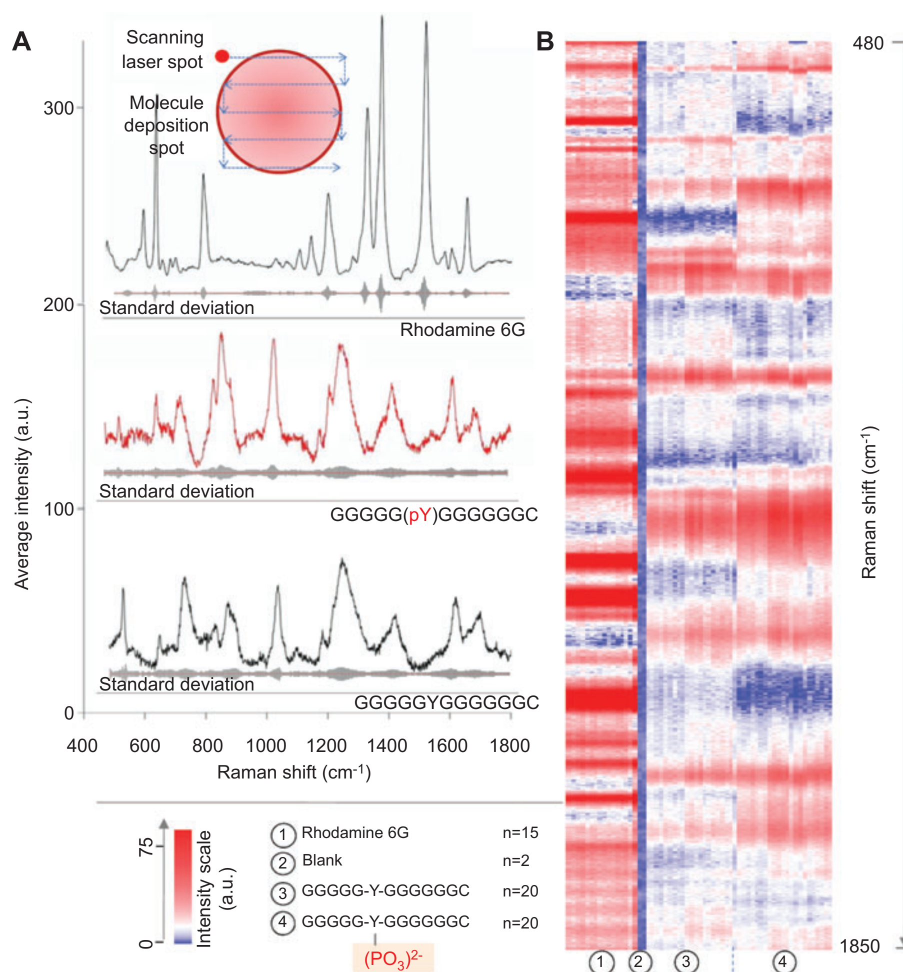

Figure 12 Uniformity testing of low concentration molecule deposition by SERS [147]. (A) Averaged spectra and standard deviations of 2D laser scanning SERS spectroscopy measurements over the deposition spots of 100 nM R6G molecules, peptides, and phosphor-peptides. The averaged spectra are the arithmetic average of all the SERS spectra acquired from each individual deposition spot. (B) Color-coded representation of multiple scanning SERS spectra from the molecule deposition spots. Raw SERS spectra obtained from either R6G (spectra number, n=15), peptides (n=20), phosphor-peptides (n=20), or blank area are shown. Normalized (intensity=0–100) SERS spectral intensities are converted using a color scale ranging from blue (intensity=0) to white (intensity=10) to red (intensity >75), and linearly represented (from 480 to 1850 cm^{-1}). Color-coding of spectra allows side-by-side representation of all datasets for rapid visual assertion of similarities and/or differences to assess the molecule deposition uniformity.

(Verigene ID™, Nanosphere Inc, Northbrook, IL, USA). At various exposure times, each microarray is scanned multiple times. As a result, this system can genotype multiple genes in the same sample in approximately 1 h with as little as 500 ng of input genomic DNA (comparable to the amount present in a single drop of blood).

6. Conclusion

Plasmonic nanobiosensors are built on the synergetic combination of plasmonic nanostructures, plasmonics, and surface biofunctionalization. The resonant EM behavior of noble-metal NPs, so-called plasmonic behavior, is due to the confinement of the conduction electrons to the small particle volume. Exquisitely controlled synthesis and fabrication of plasmonic nanostructures are combined with advances in theory and the emergence of quantitative EM modeling tools. This combination provides an increased understanding of the optical properties of isolated and electromagnetically coupled nanostructures of various sizes and shapes. This increased understanding of plasmonics enables us to more effectively design and synthesize plasmonic nanostructures that fit the need of different applications. Plasmonic nanostructures offer a highly sensitive response to the dielectric change of the environments within tens of nanometers from nanomaterials surface. Surface biofunctionalization integrated unique recognition properties of bioreceptors with unique optical properties of plasmonic nanostructures to make the originally non-specific but sensitive dielectric response specific to the analyte of interest. Furthermore, the bioreceptors (e.g., enzymes, antigens, and antibodies) have dimensions in the range of 2–20 nm, similar to those of nanostructures, indicating that the two classes of materials are structurally compatible. The size of the bioreceptors

Brought to you by | University of California - Berkeley (University of California - Berkeley)
Authenticated | 172.16.1.226
Download Date | 7/6/12 12:05 PM

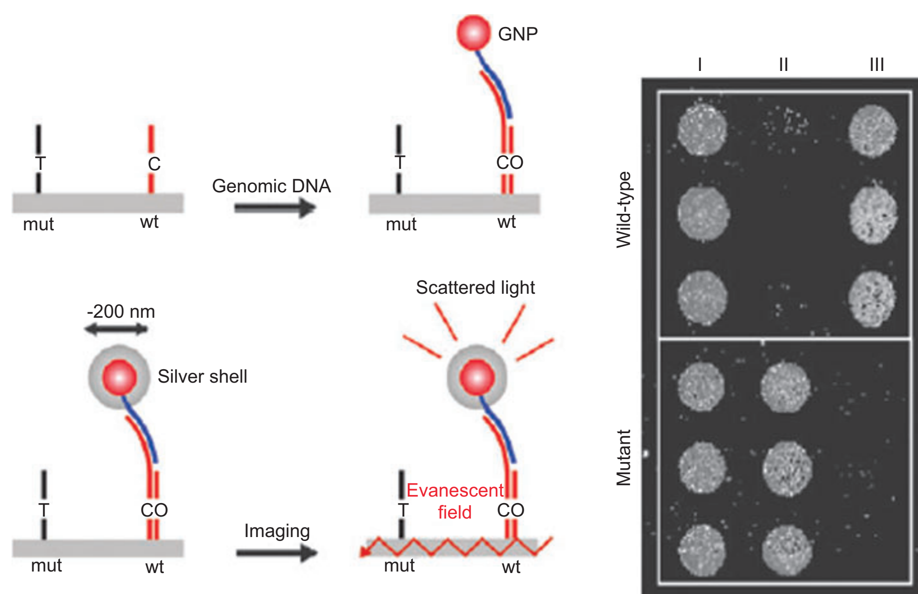

Figure 13 (A) Schematic protocol for single nanoparticle (SNP) identification in the Verigene system (Nanosphere Inc, Northbrook, IL, USA). Genomic DNA is contacted with a microarray of allele-specific capture probes. After removing unbound DNA, hybridization products are labeled with gold nanoparticles (GNPs). The GNPs are coated by silver shell, enhancing the signal (the scattering light) that is imaged in the Verigene ID™ imaging system. (B) 16-Bit grayscale images are created by the Verigene ID™ imaging system after genomic DNA samples of known genotype [(I) heterozygous, (II) homozygous wild-type, (III) homozygous mutant] were subjected to a 1-h assay. Array image reprinted from [150] with permission from Oxford University Press.

also dictates the low limit on the minimum size of plasmonic nanomaterials for biosensing. The nanosize of both bioreceptors and nanostructures made highly miniaturized signal transducers possible, whereas multiplex, real-time, and parallel sensing can be achieved by combining the highly tunable size, shape, structures, and composition of plasmonic nanostructures with a wide variety of available bioreceptors and rapid development of surface biofunctionalization strategies.

This synergetic combination of plasmonic nanostructures, plasmonics, and surface biofunctionalization offers plasmonic nanobiosensors the attractive advantages over other biosensors to better address the major challenges previously mentioned in biosensing. First and foremost, plasmonic nanobiosensors have tunable optical properties to fit a wide variety of applications. The frequency and intensity of the nanoparticle LSPR extinction or scattering bands are highly sensitive to size, shape, orientation, composition, and structure (e.g., shell-core structure) of the NPs, as well as the local dielectric environments, which reduce or eliminate amplification procedures. Therefore, the LSPR can be tuned during fabrication by controlling these parameters with a variety of chemical synthesis and nanofabrication techniques. The nanoparticle array-based biosensors can also be transitioned to single NPs to improve LSPR sensitivity to the level of a single molecule. In addition, plasmonic nanobiosensors possess greater spatial resolution, both lateral and normal, compared with SPR. The ultimate lateral spatial resolution is achieved with single NPs. Plasmonic nanobiosensors have an inherent advantage of the label-free nature over other optical biosensors that require organic fluorescent dyes and/or inorganic agents such as quantum dots to transduce the binding event because the measured quantity is the optical response of the metal. The label-free nature can significantly reduce sample preparation procedures for biosensing. Moreover, unlike fluorophores, plasmonic NPs do not blink or bleach, providing a virtually unlimited photon budget for observing molecular binding over arbitrarily long time intervals, which makes long-term continuous biosensing possible. Moreover, observation of local surface plasmons can be done using simple and inexpensive spectrophotometric equipment in the transmission (or reflection) configuration, which is important for fabricating a large biosensing array that consists of thousands of biosensors.

In conclusion, from a speculative viewpoint, the field will evolve in 5–10 years time mainly in the following directions: (i) plasmonic nanoresonance sensors with much higher sensitivity than conventional plasmonic resonance biosensors; (ii) plasmonic sensor devices made by advanced nanomanufacturing methods; (iii) beyond the molecular level, advances in complex system and detection background such as cellular, intracellular, and tissue-level detection with plasmonic coupling devices; (iv) functional genomics and proteomic sensing by plasmonic and SERS devices; (v) combination of current plasmonic nanomaterials with other nanomaterials such as quantum dots and metamaterials to improve the tunability and sensitivity and enable new synergized advantages; (vi) combination of different plasmonic sensing techniques such as SERS and LSPR; (vii) overcome the challenges in using LSPR sensing as a laboratory tool for molecular biology; and (viii) overcome the challenges in using LSPR sensing as a medical diagnostic tool.

Brought to you by | University of California - Berkeley (University of California - Berkeley)
Authenticated | 172.16.1.226
Download Date | 7/6/12 12:05 PM

7. Executive summary

- Plasmon-resonant nano-bio hybrids, so-called plasmonic nanobiosensors, synergize three core techniques: (i) plasmonics that manipulate light at nanoscale dielectric-metal interfaces for high sensitivity due to the resulting surface-enhanced light; (ii) nanofabrication and controlled synthesis of nanomaterials containing metals (e.g., Ag and Au) for high tenability; and (iii) bioconjugates techniques for high selectivity.
- Plasmonic nanobiosensors are being developed and viewed as one key breakthrough area to address these major challenges in biosensing research and personalized medicine: real-time and parallelized biomedical analysis with high selectivity and sensitivity.
- Surface plasmons include non-propagating LSPs and propagating SPPs. Both are essential for surface-enhanced biosensing techniques such as SEF, SPR, LSRP, SERS, and SEIRS.
- Current fabrication methods for LSPR and SERS substrates typically rely on bottom-up nanostructure synthesis, top-down nanostructure fabrication, or combinations of both processes to achieve the well-control of the size, shape, composition, and configuration of plasmonic nanostructures.
- Surface functionalization techniques of nanomaterials by biological recognition elements have recently been developed to incorporate the highly selective catalytic and recognition properties of biomaterials into plasmonic nanobiosensors.
- Future perspectives.

Acknowledgments

This work was funded by a generous gift from the Agilent Foundation, NIEHS grant 1RC2ES018812-01, National Natural Science Foundation of China Grant NSFC-30828010, DOD grant W81XWH-07-1-0663_BC061995, U.S. DOE contract DE-AC03-76SF00098, DARPA and MEMS fundamental science program.

References

[1] Spiller DG, Wood CD, Rand DA, White MR. Measurement of single-cell dynamics. *Nature* 2010, 465, 736–745.
[2] Anker JN, Hall WP, Lyandres O, Shah NC, Zhao J, Van Duyne RP. Biosensing with plasmonic nanosensors. *Nat. Mater.* 2008, 7, 442–453.
[3] Lal S, Link S, Halas NJ. Nano-optics from sensing to waveguiding. *Nat. Photonics* 2007, 1, 641–648.
[4] Nguyen T, Hilton JP, Lin Q. Emerging applications of aptamers to micro- and nanoscale biosensing. *Microfluid. Nanofluid.* 2009, 6, 347–362.
[5] O'Sullivan CK. Aptasensors – the future of biosensing. *Anal. Bioanal. Chem.* 2002, 372, 44–48.
[6] Ge Y, Turner AP. Too large to fit? Recent developments in macromolecular imprinting. *Trends Biotechnol.* 2008, 26, 218–224.
[7] Lu XM, Rycenga M, Skrabalak SE, Wiley B, Xia YN. Chemical synthesis of novel plasmonic nanoparticles. *Annu. Rev. Phys. Chem.* 2009, 60, 167–192.
[8] Stewart ME, Anderton CR, Thompson LB, Maria J, Gray SK, Rogers JA, Nuzzo RG. Nanostructured plasmonic sensors. *Chem. Rev.* 2008, 108, 494–521.
[9] Xia YN, Halas NJ. Shape-controlled synthesis and surface plasmonic properties of metallic nanostructures. *MRS Bull.* 2005, 30, 338–344.
[10] Zhao J, Pinchuk AO, McMahon JM, Li S, Ausman LK, Atkinson AL, Schatz GC. Methods for describing the electromagnetic properties of silver and gold nanoparticles. *Acc. Chem. Res.* 2008, 41, 1710–1720.
[11] Pitarke JM, Silkin VM, Chulkov EV, Echenique PM. Theory of surface plasmons and surface-plasmon polaritons. *Rep. Prog. Phys.* 2007, 70, 1–87.
[12] Prodan E, Radloff C, Halas NJ, Nordlander P. A hybridization model for the plasmon response of complex nanostructures. *Science* 2003, 302, 419–422.
[13] Thanh N, Green L. Functionalisation of nanoparticles for biomedical applications. *Nano Today* 2010, 5, 213–230.
[14] Geneviève M, Vieu C, Carles R, Zwick A, Brière G, Salomé L, Trévisiol E. Biofunctionalization of gold nanoparticles and their spectral properties. *Microelectron. Eng.* 2007, 84, 1710–1713.
[15] Wang CG, Ma ZF, Wang TT, Su ZM. Synthesis, assembly, and biofunctionalization of silica-coated gold nanorods for colorimetric biosensing. *Adv. Funct. Mater.* 2006, 16, 1673–1678.
[16] Sepulveda B, Angelome PC, Lechuga LM, Liz-Marzan LM. LSPR-based nanobiosensors. *Nano Today* 2009, 4, 244–251.
[17] Willets KA, Van Duyne RP. Localized surface plasmon resonance spectroscopy and sensing. *Annu. Rev. Phys. Chem.* 2007, 58, 267–297.
[18] Wachsmann-Hogiu S, Weeks T, Huser T. Chemical analysis in vivo and in vitro by Raman spectroscopy – from single cells to humans. *Curr. Opin. Biotechnol.* 2009, 20, 63–73.
[19] Stiles PL, Dieringer JA, Shah NC, Van Duyne RR. Surface-enhanced Raman spectroscopy. *Annu. Rev. Anal. Chem.* 2008, 1, 601–626.
[20] Choi YH, Kang T, Lee LP. Plasmon resonance energy transfer (PRET)-based molecular imaging of cytochrome c in living cells. *Nano Lett.* 2009, 9, 85–90.
[21] Choi Y, Park Y, Kang T, Lee LP. Selective and sensitive detection of metal ions by plasmonic resonance energy transfer-based nanospectroscopy. *Nat. Nanotechnol.* 2009, 4, 742–746.
[22] Liu GL, Long YT, Choi Y, Kang T, Lee LP. Quantized plasmon quenching dips nanospectroscopy via plasmon resonance energy transfer. *Nat. Methods* 2007, 4, 1015–1017.
[23] Kim JW, Galanzha EI, Shashkov EV, Moon HM, Zharov VP. Golden carbon nanotubes as multimodal photoacoustic and photothermal high-contrast molecular agents. *Nat. Nanotechnol.* 2009, 4, 688–694.
[24] National Research Council (U.S.); Committee on Nanophotonics Accessibility and Applicability. *Nanophotonics: Accessibility and Applicability*, National Academies Press: Washington, DC, 2008.
[25] Maier SA. *Plasmonics: Fundamentals and Applications*, Springer: New York, 2007.
[26] Le Ru, EC, Etchegoin, PG. *Principles of Surface-enhanced Raman Spectroscopy: and Related Plasmonic Effects*, 1st ed., Elsevier: Amsterdam, 2009, p. 688.
[27] Liu GL, Yin Y, Kunchakarra S, Mukherjee B, Gerion D, Jett SD, Bear DG, Gray JW, Alivisatos AP, Lee LP, Chen FF. A nanoplasmonic molecular ruler for measuring nuclease activity and DNA footprinting. *Nat. Nanotechnol.* 2006, 1, 47–52.
[28] Brockman JM, Nelson BP, Corn RM. Surface plasmon resonance imaging measurements of ultrathin organic films. *Annu. Rev. Phys. Chem.* 2000, 51, 41–63.

Brought to you by | University of California - Berkeley (University of California - Berkeley)
Authenticated | 172.16.1.226
Download Date | 7/6/12 12:05 PM

[29] Knoll W. Interfaces and thin films as seen by bound electromagnetic waves. *Annu. Rev. Phys. Chem.* 1998, 49, 569–638.
[30] Barnes WL, Dereux A, Ebbesen TW. Surface plasmon subwavelength optics. *Nature* 2003, 424, 824–830.
[31] Moskovits M. Surface-enhanced spectroscopy. *Rev. Mod. Phys.* 1985, 57, 783–826.
[32] Jackson JD. *Classical Electrodynamics*, 3rd ed., Wiley: New York, 1999.
[33] Johnson PB, Christy RW. Optical-constants of noble-metals. *Phys. Rev. B* 1972, 6, 4370–4379.
[34] Bohren CF, Huffman DR. *Absorption and Scattering of Light by Small Particles*, Wiley-VCH: New York, 1998.
[35] Haes AJ, Van Duyne RP. A unified view of propagating and localized surface plasmon resonance biosensors. *Anal. Bioanal. Chem.* 2004, 379, 920–930.
[36] Jung LS, Campbell CT, Chinowsky TM, Mar MN, Yee SS. Quantitative interpretation of the response of surface plasmon resonance sensors to adsorbed films. *Langmuir* 1998, 14, 5636–5648.
[37] Haes AJ, Van Duyne RP. A nanoscale optical biosensor: sensitivity and selectivity of an approach based on the localized surface plasmon resonance spectroscopy of triangular silver nanoparticles. *J. Am. Chem. Soc.* 2002, 124, 10596–10604.
[38] Mcfarland AD, Van Duyne RP. Single silver nanoparticles as real-time optical sensors with zeptomole sensitivity. *Nano Lett.* 2003, 3, 1057–1062.
[39] Raschke G, Kowarik S, Franzl T, Sönnichsen C, Klar TA, Feldmann J, Nichtl A, Kürzinger K. Biomolecular recognition based on single gold nanoparticle light scattering. *Nano Lett.* 2003, 3, 935–938.
[40] Kneipp K. Surface-enhanced Raman scattering. *Phys. Today* 2007, 60, 40–46.
[41] Ataka K, Heberle J. Biochemical applications of surface-enhanced infrared absorption spectroscopy. *Anal. Bioanal. Chem.* 2007, 388, 47–54.
[42] Adato R, Yanik AA, Amsden JJ, Kaplan DL, Omenetto FG, Hong MK, Erramilli S, Altug H. Ultra-sensitive vibrational spectroscopy of protein monolayers with plasmonic nanoantenna arrays. *Proc. Natl. Acad. Sci. USA* 2009, 106, 19227–19232.
[43] Fort E, Gresillon S. Surface enhanced fluorescence. *J. Phys. D Appl. Phys.* 2008, 41, 1–31.
[44] Fleischm M, Hendra PJ, Mcquilla AJ. Raman-spectra of pyridine adsorbed at a silver electrode. *Chem. Phys. Lett.* 1974, 26, 163–166.
[45] Jeanmaire DL, Vanduyne RP. Surface Raman spectroelectrochemistry. 1. Heterocyclic, Aromatic, and aliphatic-amines adsorbed on anodized silver electrode. *J. Electroanal. Chem.* 1977, 84, 1–20.
[46] Albrecht MG, Creighton JA. Anomalously intense Raman-spectra of pyridine at a silver electrode. *J. Am. Chem. Soc.* 1977, 99, 5215–5217.
[47] Aroca R. *Surface-enhanced Vibrational Spectroscopy*, Wiley: Chichester, 2006.
[48] Kneipp K, Moskovits M, Kneipp H. Surface-enhanced Raman Scattering: Physics and Applications, Springer: Berlin, 2006.
[49] Lee SE, Lee LP. Biomolecular plasmonics for quantitative biology and nanomedicine. *Curr. Opin. Biotechnol.* 2010, 21, 489–497.
[50] Liu GL. Nanoplasmonic-particle-enhanced optical molecular sensing. *Select. Top. Quant. Electron. IEEE J.* 2010, 16, 662–671.
[51] Gersten J, Nitzan A. Electromagnetic theory of enhanced Raman scattering by molecules adsorbed on rough surfaces. *J. Chem. Phys.* 1980, 73, 3023–3037.
[52] Burda C, Chen X, Narayanan R, El-Sayed MA. Chemistry and properties of nanocrystals of different shapes. *Chem. Rev.* 2005, 105, 1025–1102.
[53] Xia Y, Xiong Y, Lim B, Skrabalak SE. Shape-controlled synthesis of metal nanocrystals: simple chemistry meets complex physics. *Angew. Chem. Int. Ed.* 2009, 48, 60–103.
[54] Grabar KC, Freeman RG, Hommer MB, Natan MJ. Preparation and characterization of Au colloid monolayers. *Anal. Chem.* 1995, 67, 735–743.
[55] Wiley B, Herricks T, Sun YG, Xia YN. Polyol synthesis of silver nanoparticles: use of chloride and oxygen to promote the formation of single-crystal, truncated cubes and tetrahedrons. *Nano Lett.* 2004, 4, 1733–1739.
[56] Sun Y, Mayers B, Xia Y. Metal nanostructures with hollow interiors. *Adv. Mater.* 2003, 15, 641–646.
[57] Tao AR, Habas S, Yang P. Shape control of colloidal metal nanocrystals. *Small* 2008, 4, 310–325.
[58] Wiley BJ, Im SH, Li ZY, Mclellan J, Siekkinen A, Xia YA. Maneuvering the surface plasmon resonance of silver nanostructures through shape-controlled synthesis. *J. Phys. Chem. B* 2006, 110, 15666–15675.
[59] Washio I, Xiong YJ, Yin YD, Xia YN. Reduction by the end groups of poly(vinyl pyrrolidone): a new and versatile route to the kinetically controlled synthesis of Ag triangular nanoplates. *Adv. Mater.* 2006, 18, 1745–1749.
[60] Jackson JB, Halas NJ. Silver nanoshells: variations in morphologies and optical properties. *J. Phys. Chem. B* 2001, 105, 2743–2746.
[61] Halas N. Playing with plasmons: tuning the optical resonant properties of metallic nanoshells. *MRS Bull.* 2005, 30, 362–367.
[62] Svoboda K, Block SM. Biological applications of optical forces. *Annu. Rev. Biophys. Biomol. Struct.* 1994, 23, 247–285.
[63] Wang H, Brandl DW, Le F, Nordlander P, Halas NJ. Nanorice: a hybrid plasmonic nanostructure. *Nano Lett.* 2006, 6, 827–832.
[64] Grzelczak M, Perez-Juste J, Mulvaney P, Liz-Marzan LM. Shape control in gold nanoparticle synthesis. *Chem. Soc. Rev.* 2008, 37, 1783–1791.
[65] Barbosa S, Agrawal A, Rodriguez-Lorenzo L, Pastoriza-Santos I, Alvarez-Puebla RA, Kornowski A, Weller H, Liz-Marzán LM. Tuning size and sensing properties in colloidal gold nanostars. *Langmuir* 2010, 26, 14943–14950.
[66] Nikoobakht B, El-Sayed MA. Preparation and growth mechanism of gold nanorods (NRs) using seed-mediated growth method. *Chem. Mater.* 2003, 15, 1957–1962.
[67] Lin Y, Zou Y, Mo Y, Guo J, Lindquist RG. E-Beam patterned gold nanodot arrays on optical fiber tips for localized surface plasmon resonance biochemical sensing. *Sensors-Basel* 2010, 10, 9397–9406.
[68] Fu Y, Bryan N. Investigation of physical properties of quartz after focused ion beam bombardment. *Appl. Phys. B* 2005, 80, 581–585.
[69] Hutter E, Fendler JH. Exploitation of localized surface plasmon resonance. *Adv. Mater.* 2004, 16, 1685–1706.
[70] David C, Guillot N, Shen H, Toury T, Lamy De La Chapelle M. SERS detection of biomolecules using lithographed nanoparticles towards a reproducible SERS biosensor. *Nanotechnology* 2010, 21, 475501.
[71] Tripp RA, Dluhy RA, Zhao Y. Novel nanostructures for SERS biosensing. *Nano Today* 2008, 3, 31–37.
[72] De Jesus MA, Giesfeldt KS, Oran JM, Abu-Hatab NA, Lavrik NV, Sepaniak MJ. Nanofabrication of densely packed metal-polymer arrays for surface-enhanced Raman spectrometry. *Appl. Spectrosc.* 2005, 59, 1501–1508.

Brought to you by | University of California - Berkeley (University of California - Berkeley)
Authenticated | 172.16.1.226
Download Date | 7/6/12 12:05 PM

[73] Camden JP, Dieringer JA, Zhao J, Van Duyne RP. Controlled plasmonic nanostructures for surface-enhanced spectroscopy and sensing. *Acc. Chem. Res.* 2008, 41, 1653–1661.
[74] Haynes CL, Van Duyne RP. Plasmon-sampled surface-enhanced Raman excitation spectroscopy. *J. Phys. Chem. B* 2003, 107, 7426–7433.
[75] Mcfarland AD, Young MA, Dieringer JA, Van Duyne RP. Wavelength-scanned surface-enhanced Raman excitation spectroscopy. *J. Phys. Chem. B* 2005, 109, 11279–11285.
[76] Haynes CL, Mcfarland AD, Smith MT, Hulteen JC, Van Duyne RP. Angle-resolved nanosphere lithography: manipulation of nanoparticle size, shape, and interparticle spacing. *J. Phys. Chem. B* 2002, 106, 1898–1902.
[77] Rybczynski J, Ebels U, Giersig M. Large-scale, 2D arrays of magnetic nanoparticles. *Colloids Surf. Physicochem. Eng. Aspects* 2003, 219, 1–6.
[78] Du Y, Shi L, He T, Sun X, Mo Y. SERS enhancement dependence on the diameter and aspect ratio of silver-nanowire array fabricated by anodic aluminium oxide template. *Appl. Surf. Sci.* 2008, 255, 1901–1905.
[79] Ruan C, Eres G, Wang W, Zhang Z, Gu B. Controlled fabrication of nanopillar arrays as active substrates for surface-enhanced Raman spectroscopy. *Langmuir* 2007, 23, 5757–5760.
[80] Jung D, Lee YM, Lee Y, Kim NH, Kim K, Lee J-K. Facile fabrication of large area nanostructures for efficient surface-enhanced Raman scattering. *J. Mater. Chem.* 2006, 16, 3145–3149.
[81] Driskell JD, Shanmukh S, Liu Y, Chaney SB, Tang XJ, Zhao YP, Dluhy RA. The use of aligned silver nanorod arrays prepared by oblique angle deposition as surface enhanced Raman scattering substrates. *J. Phys. Chem. C* 2008, 112, 895–901.
[82] Chaney SB, Shanmukh S, Dluhy RA, Zhao YP. Aligned silver nanorod arrays produce high sensitivity surface-enhanced Raman spectroscopy substrates. *Appl. Phys. Lett.* 2005, 87, 031908.
[83] Zhou Q, Li Z, Yang Y, Zhang Z. Arrays of aligned, single crystalline silver nanorods for trace amount detection. *J. Phys. D Appl. Phys.* 2008, 41, 152007.
[84] Dickey MD, Weiss EA, Smythe EJ, Chiechi RC, Capasso F, Whitesides GM. Fabrication of arrays of metal and metal oxide nanotubes by shadow evaporation. *ACS Nano* 2008, 2, 800–808.
[85] Madou MJ. *Fundamentals of Microfabrication: The Science of Miniaturization*, 2nd ed., CRC Press: Boca Raton, FL, 2002.
[86] Li K, Clime L, Tay L, Cui B, Geissler M, Veres T. Multiple surface plasmon resonances and near-infrared field enhancement of gold nanowells. *Anal. Chem.* 2008, 80, 4945–4950.
[87] Clark AW, Cooper JM. Nanogap ring antennae as plasmonically coupled SERRS substrates. *Small* 2011, 7, 119–125.
[88] Chou SY, Krauss PR, Renstrom PJ. Imprint of sub-25 nm vias and trenches in polymers. *Appl. Phys. Lett.* 1995, 67, 3114–3116.
[89] Chou SY, Krauss PR, Renstrom PJ. Nanoimprint lithography. *J. Vac. Sci. Technol. B* 1996, 14, 4129–4133.
[90] Lucas BD, Kim J-S, Chin C, Guo LJ. Nanoimprint lithography based approach for the fabrication of large-area, uniformly-oriented plasmonic arrays. *Adv. Mater.* 2008, 20, 1129–1134.
[91] Alvarez-Puebla R, Cui B, Bravo-Vasquez J-P, Veres T, Fenniri H. Nanoimprinted SERS-active substrates with tunable surface plasmon resonances. *J. Phys. Chem. C* 2007, 111, 6720–6723.
[92] Lee S-W, Lee K-S, Ahn J, Lee J-J, Kim M-G, Shin Y-B. Highly sensitive biosensing using arrays of plasmonic Au nanodisks realized by nanoimprint lithography. *ACS Nano* 2011, 5, 897–904.
[93] Guo LJ. Nanoimprint lithography: methods and material requirements. *Adv. Mater.* 2007, 19, 495–513.
[94] Masuda H, Fukuda K. Ordered metal nanohole arrays made by a two-step replication of honeycomb structures of anodic alumina. *Science* 1995, 268, 1466–1468.
[95] Lei Y, Yang S, Wu M, Wilde G. Surface patterning using templates: concept, properties and device applications. *Chem. Soc. Rev.* 2011, 40, 1247–1258.
[96] Broglin BL, Andreu A, Dhussa N, Heath JA, Gerst J, Dudley B, Holland D, El-Kouedi M. Investigation of the effects of the local environment on the surface-enhanced Raman spectra of striped gold/silver nanorod arrays. *Langmuir* 2007, 23, 4563–4568.
[97] Bok H-M, Shuford KL, Kim S, Kim SK, Park S. Multiple surface plasmon modes for a colloidal solution of nanoporous gold nanorods and their comparison to smooth gold nanorods. *Nano Lett.* 2008, 8, 2265–2270.
[98] Choi D, Choi Y, Hong S, Kang T, Lee LP. Self-organized hexagonal-nanopore SERS array. *Small* 2010, 6, 1741–1744.
[99] Qin Y, Pan A, Liu L, Moutanabbir O, Yang RB, Knez M. Atomic layer deposition assisted template approach for electrochemical synthesis of Au crescent-shaped half-nanotubes. *ACS Nano* 2011, 5, 788–794.
[100] Bang J, Jeong U, Ryu DY, Russell TP, Hawker CJ. Block copolymer nanolithography: translation of molecular level control to nanoscale patterns. *Adv. Mater.* 2009, 21, 4769–4792.
[101] Kim SO, Solak HH, Stoykovich MP, Ferrier NJ, De Pablo JJ, Nealey PF. Epitaxial self-assembly of block copolymers on lithographically defined nanopatterned substrates. *Nature* 2003, 424, 411–414.
[102] Cheng JY, Mayes AM, Ross CA. Nanostructure engineering by templated self-assembly of block copolymers. *Nat. Mater.* 2004, 3, 823–828.
[103] Deckman HW, Dunsmuir JH. Natural lithography. *Appl. Phys. Lett.* 1982,41, 377–379.
[104] Malinsky MD, Kelly KL, Schatz GC, Van Duyne RP. Nanosphere lithography: effect of substrate on the localized surface plasmon resonance spectrum of silver nanoparticles. *J. Phys. Chem. B* 2001, 105, 2343–2350.
[105] Hulteen JC, Treichel DA, Smith MT, Duval ML, Jensen TR, Van Duyne RP. Nanosphere lithography: size-tunable silver nanoparticle and surface cluster arrays. *J. Phys. Chem. B* 1999, 103, 3854–3863.
[106] Kuo C-W, Shiu J-Y, Chien F-C, Tsai S-M, Chueh D-Y, Chen P. Polymeric nanopillar arrays for cell traction force measurements. *Electrophoresis* 2010, 31, 3152–3158.
[107] Masson J-F, Murray-Methot M-P, Live LS. Nanohole arrays in chemical analysis: manufacturing methods and applications. *Analyst* 2010, 135, 1483–1489.
[108] Peng K, Zhang M, Lu A, Wong N-B, Zhang R, Lee S-T. Ordered silicon nanowire arrays via nanosphere lithography and metal-induced etching. *Appl. Phys. Lett.* 2007, 90, 163123.
[109] Xu M, Lu N, Xu H, Qi D, Wang Y, Chi L. Fabrication of functional silver nanobowl arrays via sphere lithography. *Langmuir* 2009, 25, 11216–11220.
[110] Aizpurua J, Hanarp P, Sutherland DS, Kall M, Bryant GW, Garcia De Abajo FJ. Optical properties of gold nanorings. *Phys. Rev. Lett.* 2003, 90, 057401.
[111] Vossen DLJ, Fific D, Penninkhof J, Van Dillen T, Polman A, Van Blaaderen A. Combined optical tweezers/ion beam technique to tune colloidal masks for nanolithography. *Nano Lett.* 2005, 5, 1175–1179.

Brought to you by | University of California - Berkeley (University of California - Berkeley)
Authenticated | 172.16.1.226
Download Date | 7/6/12 12:05 PM

[112] Jiang P, Mcfarland MJ. Wafer-scale periodic nanohole arrays templated from two-dimensional nonclose-packed colloidal crystals. *J. Am. Chem. Soc.* 2005, 127, 3710–3711.
[113] Masson J-F, Gibson KF, Provencher-Girard A. Surface-enhanced Raman spectroscopy amplification with film over etched nanospheres. *J. Phys. Chem. C* 2010, 114, 22406–22412.
[114] Haynes CL, Van Duyne RP. Nanosphere lithography: a versatile nanofabrication tool for studies of size-dependent nanoparticle optics. *J. Phys. Chem. B* 2001, 105, 5599–5611.
[115] Burmeister F, Schafle C, Matthes T, Bohmisch M, Boneberg J, Leiderer P. Colloid monolayers as versatile lithographic masks. *Langmuir* 1997, 13, 2983–2987.
[116] Hawkeye MM, Brett MJ. Glancing angle deposition: fabrication, properties, and applications of micro- and nanostructured thin films. *J. Vac. Sci. Technol. A* 2007, 25, 1317–1335.
[117] Steele JJ, Brett MJ. Nanostructure engineering in porous columnar thin films: recent advances. *J. Mater. Sci. Mater. Electron* 2007, 18, 367–379.
[118] Brett MJ, Hawkeye MM. New materials at a glance. *Science* 2008, 319, 1192–1193.
[119] Jensen MO, Brett MJ. Periodically structured glancing angle deposition thin films. *Nanotechnol. IEEE Trans.* 2005, 4, 269–277.
[120] Huang ZF, Harris KD, Brett MJ. Morphology control of nanotube arrays. *Adv. Mater.* 2009, 21, 2983–2987.
[121] Fu J, Zhao Y. Optical properties of silver/gold nanostructures fabricated by shadowing growth and their sensing applications. *Nanostruct. Thin Films III* 2010, 7766, 77660.
[122] Zhou CM, Gall D. Surface patterning by nanosphere lithography for layer growth with ordered pores. *Thin Solid Films* 2007, 516, 433–437.
[123] Ye DX, Lu TM. Ballistic aggregation on two-dimensional arrays of seeds with oblique incident flux: growth model for amorphous Si on Si. *Phys. Rev. B* 2007, 76, 235402.
[124] Huang Z, Harris KD, Brett MJ. Morphology control of nanotube arrays. *Adv. Mater.* 2009, 21, 2983–2987.
[125] Robbie K, Brett MJ, Lakhtakia A. Chiral sculptured thin films. *Nature* 1996, 384, 616.
[126] Kennedy SR, Brett MJ, Toader O, John S. Fabrication of tetragonal square spiral photonic crystals. *Nano Lett.* 2002, 2, 59–62.
[127] Fu J, Park B, Siragusa G, Jones L, Tripp R, Zhao Y, Cho YJ. An Au/Si hetero-nanorod-based biosensor for Salmonella detection. *Nanotechnology* 2008, 19, 155502.
[128] Liu YJ, Zhang ZY, Dluhy RA, Zhao YP. The SERS response of semiordered Ag nanorod arrays fabricated by template oblique angle deposition. *J. Raman Spectrosc.* 2010, 41, 1112–1118.
[129] Wang X, Liu LH, Ramstrom O, Yan MD. Engineering nanomaterial surfaces for biomedical applications. *Exp. Biol. Med.* 2009, 234, 1128–1139.
[130] Cobley CM, Chen JY, Cho EC, Wang LV, Xia YN. Gold nanostructures: a class of multifunctional materials for biomedical applications. *Chem. Soc. Rev.* 2011, 40, 44–56.
[131] Shenton W, Davis SA, Mann S. Directed self-assembly of nanoparticles into macroscopic materials using antibody-antigen recognition. *Adv. Mater.* 1999, 11, 449–452.
[132] Naka K, Itoh H, Tampo Y, Chujo Y. Effect of gold nanoparticles as a support for the oligomerization of L-cysteine in an aqueous solution. *Langmuir* 2003, 19, 5546–5549.
[133] Hayat MA. *Colloidal Gold: Principles, Methods, and Applications*, Academic Press: San Diego, CA, 1989.
[134] Mirkin CA, Letsinger RL, Mucic RC, Storhoff JJ. A DNA-based method for rationally assembling nanoparticles into macroscopic materials. *Nature* 1996, 382, 607–609.
[135] Sonnichsen C, Reinhard BM, Liphardt J, Alivisatos AP. A molecular ruler based on plasmon coupling of single gold and silver nanoparticles. *Nat. Biotechnol.* 2005, 23, 741–745.
[136] Niemeyer CM. Nanoparticles, proteins, and nucleic acids: biotechnology meets materials science. *Angew. Chem. Int. Ed.* 2001, 40, 4128–4158.
[137] Green NM. Avidin. *Adv. Protein Chem.* 1975, 29, 85–133.
[138] Wilchek M, Bayer EA. The avidin biotin complex in bioanalytical applications. *Anal. Biochem.* 1988, 171, 1–32.
[139] Weiss S. Fluorescence spectroscopy of single biomolecules. *Science* 1999, 283, 1676–1683.
[140] Yildiz A, Forkey JN, Mckinney SA, Ha T, Goldman YE, Selvin PR. Myosin V walks hand-over-hand: single fluorophore imaging with 1.5-nm localization. *Science* 2003, 300, 2061–2065.
[141] Zhuang X, Bartley LE, Babcock HP, Russell R, Ha T, Herschlag D, Chu S. A single-molecule study of RNA catalysis and folding. *Science* 2000, 288, 2048–2051.
[142] Taton TA, Mirkin CA, Letsinger RL. Scanometric DNA array detection with nanoparticle probes. *Science* 2000, 289, 1757–1760.
[143] Yguerabide J, Yguerabide EE. Light-scattering submicroscopic particles as highly fluorescent analogs and their use as tracer labels in clinical and biological applications – II. Experimental characterization. *Anal. Biochem.* 1998, 262, 157–176.
[144] Luk'yanchuk B, Zheludev NI, Maier SA, Halas NJ, Nordlander P, Giessen H, Chong CT. The Fano resonance in plasmonic nanostructures and metamaterials. *Nat. Mater.* 2010, 9, 707–715.
[145] Yanik AA, Cetin AE, Huang M, Artar A, Mousavi SH, Khanikaev A, Connord JH, Shvetsc G, Altug H. Seeing protein monolayers with naked eye through plasmonic Fano resonances. *Proc. Natl. Acad. Sci. USA* 2011, 108, 11784–11789.
[146] Yonzon CR, Zhang XY, Van Duyne RP. Localized surface plasmon resonance immunoassay and verification using surface-enhanced Raman spectroscopy. *Proc. SPIE* 2003, 5224, 78.
[147] Coppe JP, Xu ZD, Chen Y, Liu GL. Metallic nanocone array photonic substrate for high-uniformity surface deposition and optical detection of small molecules. *Nanotechnology* 2011, 22, 245710.
[148] Storhoff JJ, Marla SS, Bao P, Hagenow S, Mehta H, Lucas A, Garimella V, Patno T, Buckingham V, Cork W, Müller UR. Gold nanoparticle-based detection of genomic DNA targets on microarrays using a novel optical detection system. *Biosens. Bioelectron.* 2004, 19, 875–883.
[149] Huber M, Wei TF, Muller UR, Lefebvre PA, Marla SS, Bao YP. Gold nanoparticle probe-based gene expression analysis with unamplified total human RNA. *Nucleic Acids Res.* 2004, 32, e137.
[150] Bao YP, Huber M, Wei TF, Marla SS, Storhoff JJ, Muller UR. SNP identification in unamplified human genomic DNA with gold nanoparticle probes. *Nucleic Acids Res.* 2005, 33, e15.

Received November 12, 2011; accepted January 26, 2012

Brought to you by | University of California - Berkeley (University of California - Berkeley)
Authenticated | 172.16.1.226
Download Date | 7/6/12 12:05 PM

Wenwei Zheng is currently a postdoctoral researcher in Electrical & Computer Engineering at University of California, San Diego, working on applications of metamaterials in biology and nanomedicine. In 2001, Wenwei received his B.Sc. in both chemistry and physics from Peking University, China. From Stanford University, he obtained his Ph.D. in Biophysical Chemistry in 2009. In 2010-2011, he was a postdoctoral researcher at University of California, Berkeley, and a postdoc scientist at Lawrence Berkeley National Laboratory, working on nanostructures of silver. His expertise lies in biomedical application of nanoplasmonic-bio hybrid materials and surface-initiated vapor deposition polymerization of polypeptides.

Heather Chiamori is currently a PhD. student at the University of California, Berkeley, in the Department of Mechanical Engineering. Her research focuses on novel synthesis platforms for nanostructured materials, including graphene, carbon nanotubes, and titanium dioxide. Through her affiliation with the Berkeley Sensor & Actuator Center, Heather has focused on device applications for chemical, electrical, and optical sensors.

Dr. Liu obtained his PhD. degree in Bioengineering from University of California-Berkeley and San Francisco in 2006. After two-year postdoctoral training in Lawrence Livermore National Laboratory, in 2008 Dr. Liu joined University of Illinois at Urbana-Champaign as a tenure-track assistant professor in the Department of Electrical and Computer Engineering, and became an affiliated faculty member in the Department of Bioengineering and the micro and nanotechnology laboratory. Dr. Liu has published over 60 journal publications, numerous conference abstracts and several book chapters. Dr. Liu's research focuses on designing and developing integrative bionano devices which allow for many innovative applications reaching various scientific fields including advanced nanomanufacturing, bioimaging, cancer diagnostics and therapy, environmental sensing and mobile health. Dr. Liu was nominated for the "CIMIT Prize in Primary Healthcare" by the national center for integration of medicine & innovative technology in 2009 and nominated for the "Damon Runyon-Rachleff Innovation Award" by Damon Runyon cancer research foundation in 2010. Dr. Liu was recipient of the "Presidential Early-Career Award for Scientists and Engineers (PECASE)" in 2011 for his research accomplishment in combining nanoengineering device research with biomolecular and cellular sensing applications.

Liwei Lin joined UC-Berkeley in 1999 and is now Professor at the Mechanical Engineering Department and co-Director at the Berkeley Sensor and Actuator Center. His research interests are in design, modeling and fabrication of micro/nano structures, micro/nano sensors and micro/nano actuators as well as mechanical issues in micro/nano systems including heat transfer, solid/fluid mechanics and dynamics. Dr. Lin is the recipient of the 1998 NSF CAREER Award for research in MEMS Packaging and the 1999 ASME Journal of Heat Transfer best paper award for his work on micro scale bubble formation. He is an ASME Fellow and has 15 issued US patents in the area of MEMS.

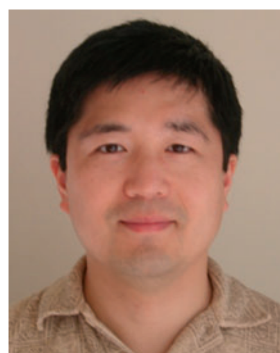

Fanqing Frank Chen is Scientist at Lawrence Berkeley National Laboratory (2000-present), Adjunct Professor at Zhejiang University's Zhejiang-California International Nanosystems Institute, and Adjunct Professor at Fudan University. He is a world leading nanobiotechnology expert and has 20+ patent and 40+ publications in high profile journals such as Nature Nanotechnology, PNAS. His advice has been sought by government agencies, by multinational corporations in multiple industries, and by Wall Street. He has given over 50 invited speeches internationally, including at Institute of Nanotechnology, Royal Society. He has led projects sponsored by DARPA, DOD, NIH, NASA, Agilent Foundation, DOE, and Chinese Natural Science Foundation. He received the Outstanding Overseas Scholarship in 2008 from the Chinese Natural Science Foundation. His patents have been commercialized by multinationals and startups into various successful products. He is editorial board member of more than half a dozen international nanotechnology journals including Nanotoxicology, Particle & Fiber Toxicology, International Journal of Computational Biosciences, and Journal of Nano Education. He has worked in Los Alamos National Laboratory (1992–1998) and NYU Mount Sinai Medical Center (1998–2000). He also performed guest scientist work at Lawrence Livermore National Laboratory, Sandia National Laboratory, and Stanford SLAC Center.

Brought to you by | University of California - Berkeley (University of California - Berkeley)
Authenticated | 172.16.1.226
Download Date | 7/6/12 12:05 PM